



Flaring efficiencies and NO_x emission ratios measured for offshore oil and gas facilities in the North Sea

Jacob T. Shaw¹, Amy Foulds¹, Shona Wilde², Patrick Barker¹, Freya Squires^{2*}, James Lee^{2,3}, Ruth Purvis^{2,3}, Ralph Burton⁴, Ioana Colfescu⁴, Stephen Mobbs⁴, Stéphane J.-B. Bauguitte⁵, Stuart Young²,
5 Stefan Schwietzke⁶, Grant Allen¹

¹Department of Earth and Environmental Sciences, University of Manchester, Oxford Road, Manchester, M13 9PL, UK

²Wolfson Atmospheric Chemistry Laboratories, Department of Chemistry, University of York, York, YO10 5DD, UK

³National Centre for Atmospheric Science, University of York, York, YO10 5DD, UK

⁴National Centre for Atmospheric Science, School of Earth and Environment, University of Leeds, Leeds, LS2 9JT, UK

10 ⁵Facility for Airborne Atmospheric Measurements FAAM 125, Cranfield University, Cranfield, UK

⁶Environmental Defense Fund, Berlin, Germany

*Now at: British Antarctic Survey, Natural Environment Research Council, Cambridge, CB3 0ET, UK

Correspondence to: Grant Allen (grant.allen@manchester.ac.uk)

Abstract. Gas flaring is a substantial global source of carbon emissions to atmosphere, and is targeted as a route to mitigating
15 the oil and gas sector carbon footprint, due to the waste of resources involved. However, quantifying carbon emissions from
flaring is resource intensive, and no studies have yet assessed flaring emissions for offshore regions. In this work, we present
carbon dioxide (CO₂), methane (CH₄), ethane (C₂H₆), and NO_x (nitrogen oxide) data from 58 emission plumes identified as
gas flaring, measured during aircraft campaigns over the North Sea (UK and Norwegian) in 2018 and 2019. Median
combustion efficiency, the efficiency with which carbon in the flared gas is converted to CO₂ in the emission plume, was
20 98.4% when accounting for C₂H₆, or 98.7% when only accounting for CH₄. Higher combustion efficiencies were measured in
the Norwegian sector of the North Sea compared with the UK sector. Destruction removal efficiencies (DREs), the efficiency
with which an individual species is combusted, were 98.5% for CH₄, and 97.9% for C₂H₆. Median NO_x emission ratios were
measured to be 0.003 ppm per ppm CO₂ and 0.26 ppm per ppm CH₄, and the median C₂H₆:CH₄ ratio was measured to be 0.11
ppm ppm⁻¹. The highest NO_x emission ratios were observed from Floating Production Storage and Offloading (FPSO) vessels,
25 although this could potentially be due to the presence of alternative NO_x sources onboard, such as diesel generators. The
measurements in this work were used to estimate total emissions from the North Sea from gas flaring, of 1.4 Tg yr⁻¹ CO₂, 6.3
Gg yr⁻¹ CH₄, 1.7 Gg yr⁻¹ C₂H₆, and 3.9 Gg yr⁻¹ NO_x.

1 Introduction

Gas flaring is a practice widely used at hydrocarbon production sites to dispose of natural gas in situations where the gas is
30 not captured for sale or used locally, and would otherwise be vented directly to atmosphere. Flaring leads to the emission of
carbon dioxide (CO₂) and short-lived climate forcers such as methane (CH₄) and black carbon (BC) (Myhre et al., 2013; Allen



et al., 2016; Fawole et al., 2016; IPCC, 2021). Ideally, all flammable gas would be fully combusted to form CO₂ as CH₄ is a much more powerful greenhouse gas (Allen et al., 2016). Flaring also results in the emission of combustion by-products, which include carbon monoxide (CO), nitrogen oxides (NO_x), and sulphur dioxide (SO₂), as well as other components of the unburned
35 fuel (such as volatile organic compounds, VOCs), which have been known to have adverse health and environmental impacts (Kahforoshan et al., 2008; Anejionu et al., 2015; EPA, 2011). The International Energy Agency (IEA) estimated that 142 × 10⁹ m³ of natural gas was flared in 2020, resulting in emissions of 265 Tg of CO₂ and 8 Tg of CH₄ (IEA, 2021). For CH₄, this represents roughly 7% of all fossil fuel related emissions, or approximately 2% of total annual anthropogenic emissions (Saunois et al., 2020). As a large source of greenhouse gas emissions (Olivier et al., 2013), reductions in gas flaring are
40 required in order to meet emission targets within the Kyoto Protocol's Clean Development Mechanism (United Nations, 1998; Elvidge et al., 2018).

Flaring is typically assumed to be highly efficient. Many inventories assume 98% of flared natural gas is converted to CO₂ (EPA, 2011; Allen et al., 2016). However, factors such as the flare volume, flare gas flow rate, or even the strength of ambient winds can affect the efficiency of flares, which can result in incomplete combustion (Johnson and Kostiuik, 2002;
45 Allen et al., 2016; Jatale et al., 2016). The IEA suggests an alternative globally averaged combustion efficiency of 92%, resulting in emissions of 500 Tg CO₂-eq in 2020 (IEA, 2021). Large uncertainties in combustion efficiencies lead to significant uncertainties in total greenhouse gas emissions from flaring (Allen et al., 2016).

There have been minimal real-world studies of flaring combustion efficiencies, with the majority focussed on test facilities and permanent flares that are subject to emission regulations (e.g. Knighton et al., 2012; Torres et al., 2012a, 2012b).
50 Flaring from oil and natural gas fields is often temporary and in-field sampling is required to gain insight into combustion efficiencies across a wide range of real operating conditions (Ismail and Umukoro, 2012). Caulton et al. (2014) measured the destruction removal efficiency (DRE) of CH₄ in 11 flared gas plumes in the Bakken Shale Formation, United States. They found that gas flares were 99.8% efficient at removing CH₄, and that wind speeds below 15 m s⁻¹ did not have an effect on their efficiency. A similar airborne study of 37 unique flares in the same Bakken region found a skewed log-normal distribution
55 of flare efficiencies, with median DREs of 97% for both CH₄ and ethane (C₂H₆) but also some flares with much lower DREs of less than 85% (Gvakharia et al. 2017). The discrepancy in flaring efficiencies measured by these two studies may be due to the targeting of larger flares (which are typically more efficient) by Caulton et al. (2014), but may also have been potentially due to the limited sample sizes. A recent study presented results from a much larger sample of over 300 unique flares measured
60 across three major oil and gas basins in the United States (Bakken Formation, Eagle Ford Shale, and Permian Basin), with mean observed DREs for CH₄ of 95.2% (Plant et al., 2022). The results exhibited a strong skewed-distribution, and, when accounting for the contribution of unlit flares (which vent CH₄ directly to atmosphere), the mean effective DRE for CH₄ was 91.1% (Plant et al., 2022).

Offshore oil and gas facilities in the North and Norwegian Seas have been the subject of several studies complementary to the work presented here. Foulds et al. (2022) measured CH₄ emission fluxes from 21 offshore facilities on
65 the Norwegian continental shelf, finding mean emissions of 211 tonnes CH₄ yr⁻¹ (6.7 g CH₄ s⁻¹) per facility. Wilde et al. (2021a)



measured much larger median CH₄ emissions of 120 g CH₄ s⁻¹ (range: 20-360 g CH₄ s⁻¹) from four facilities in the North Sea. Riddick et al. (2019) measured CH₄ emissions using a shipborne platform, reporting median emissions of 6.8 g CH₄ s⁻¹ (214 tonnes CH₄ yr⁻¹) across eight facilities, in exceptional agreement with Foulds et al. (2022). In the southern North Sea, Pühl et al. (*in prep*) measured median emissions of 10 g CH₄ s⁻¹ from a sample of UK and Dutch oil and gas platforms. However, Pühl et al. (*in prep*) also measured emissions of 350 g CH₄ s⁻¹ from a single platform, similar in magnitude to the largest emitters measured by Wilde et al. (2021a). The discrepancies between these emission flux estimates, which are often based on ‘snapshot’ studies conducted over limited timeframes, may be due to capturing different events, measuring at different lifetime phases of production, or small sample sizes. Shipborne-based measurements may also fail to capture flared emissions, as these are typically warmer than ambient air and would therefore be expected to rise in the atmosphere. The carbon isotopic signature of methane emitted from oil and gas facilities is useful for source identification, and has been measured to be -53‰ in the North Sea (Cain et al., 2017; France et al. 2021). Emissions of volatile organic compounds (VOCs) from oil and gas facilities have also been measured in the North Sea, with ratios in enhancements of C₂H₆ to CH₄ ($\Delta\text{C}_2\text{H}_6:\Delta\text{CH}_4$) measured to be between 0.03 and 0.18 ppm ppm⁻¹ (Wilde et al., 2021a; 2021b; Pühl et al., *in review*).

The volume of gas flared in the UK North Sea was reported to have fallen by 19% in 2021 (OGA, 2021). Despite this, 740 million cubic metres (7.4×10^8 m³) of natural gas were still flared (OGA, 2021), equivalent to 0.5% of gas flared globally. The UK was 23rd in the list of countries with the greatest total flaring volumes for 2020 (World Bank, 2021), with the top seven countries accounting for 65% of all flaring. The Zero Routine Flaring initiative, launched in 2015, aims to end routine gas flaring no later than 2030 and hence emissions from flaring must be monitored. Monitoring current flaring emissions from the oil and gas sector is therefore essential to robustly assess any future changes or reductions to flaring activity. In this work, we present combustion efficiencies, destruction removal efficiencies (DREs), and NO_x emission ratios calculated for a sample of flared gas plumes measured across two aircraft campaigns in the North and Norwegian Seas.



2 Methods

2.1 Atmospheric research aircraft

90 All flight measurements analysed in this work were made using the UK's Facility for Airborne Atmospheric Measurement (FAAM) BAe-146 atmospheric research aircraft. A description of the full aircraft scientific payload can be found in Palmer et al. (2018). Here, we summarise the instrumentation relevant to this study.

Meteorological and thermodynamic parameters were measured using the core instrument suite onboard the FAAM aircraft. A Rosemount 102 Total Air Temperature probe measured air temperature with an estimated uncertainty of ± 0.1 K.
95 Static pressure was measured using a series of pitot tubes (uncertainty ± 0.5 hPa) and a nose-mounted five-port turbulence probe measured three-dimensional wind components (uncertainty ± 0.5 m s⁻¹).

Dry mole fractions of CO₂ and CH₄ were measured using a cavity enhanced absorption spectrometer (Fast Greenhouse Gas Analyzer (FGGA); Los Gatos Research Inc., USA), sampling air through a window-mounted rear-facing chemistry inlet. A full description of the FGGA for measurements onboard the FAAM aircraft was reported by O'Shea et al. (2013), with a
100 modified instrumental setup (used after January 2019) described by Shaw et al. (2022). Raw CO₂ and CH₄ mole fraction data were corrected for small effects associated with water vapour dilution and spectroscopic error. Calibration was performed approximately hourly during flights, using two reference calibration gas cylinders (encapsulating a representative range of background and in-plume mole fractions) traceable to the WMO-X2007 scale for CO₂ (Tans et al., 2009) and the WMO-X2004A scale for CH₄ (Dlugokencky et al., 2005). A target reference gas cylinder was also sampled hourly to quantify small
105 sources of instrumental drift and non-linearity, and to define measurement error. For a full description of data correction, calibration and validation, refer to O'Shea et al. (2013) and Pitt et al. (2019). CH₄ and CO₂ data were measured at 1 Hz for flights conducted in 2018, and at 10 Hz for flights conducted in 2019 (Foulds et al., 2022; Shaw et al., 2022). 10 Hz measurements were time-averaged onto a 1 Hz grid for consistency between datasets. The representative one standard deviation (1σ) measurement uncertainties were ± 2.86 ppb CH₄ and ± 0.46 ppm CO₂ at a sampling rate of 1 Hz, and ± 3.23 ppb CH₄ and
110 ± 0.72 ppm CO₂, at 10 Hz.

Ethane (C₂H₆) mole fractions were measured using a tunable infrared laser direct absorption spectrometer (TILDAS, Aerodyne Research Inc.), operating at 1 Hz in the mid-infrared region ($\lambda = 3.3$ μ m). Raw C₂H₆ mole fraction data were corrected for spectroscopic effects associated with water vapour using the method described by Pitt et al. (2016). Calibration was performed using two gas standards (encapsulating a range of mole fractions) certified by the Swiss Federal Laboratories
115 for Materials Science and Technology (EMPA). The TILDAS instrument has a reported precision of ± 50 ppt over a 10 s averaging period. Two levels of data quality were provided for the C₂H₆ dataset. The "high quality" data included data that were calibrated at a stable altitude to account for systematic biases from optical effects (see Pitt et al., 2016). The "reduced quality" data included regular linear calibration (at ~ 45 minute intervals) but included data where calibration was not possible at a stable altitude. However, as we use enhanced C₂H₆ mole fractions (background subtracted) in this work, the systematic
120 altitude-dependent biases were effectively removed, and the "reduced quality" C₂H₆ data was considered acceptable.



125 Nitrogen monoxide (NO) and nitrogen dioxide (NO₂) were measured using a custom-built chemiluminescence instrument (Air Quality Design Inc.; see Graham et al., 2020 and Lee et al., 2009 for detail). NO₂ was measured on a secondary channel following photolytic conversion to NO using a blue light converter (395 nm), and subsequent detection via chemiluminescence. In-flight calibrations were performed frequently using a small flow of NO calibration gas (5 ppm NO in N₂). Estimated accuracies were ±4% for NO and ±5% for NO₂, with precisions of 31 and 45 pptv for NO and NO₂ respectively at 1 Hz. NO and NO₂ mole fractions below the instrument detection limit of 30 pptv were removed.

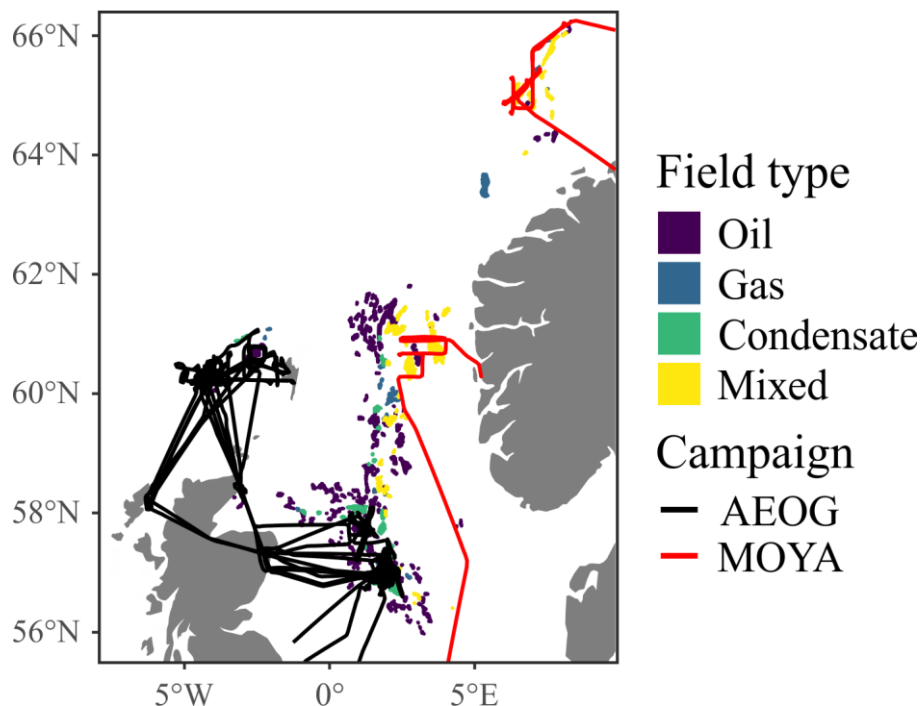
All instrumentation on board the FAAM aircraft were synchronised with respect to time prior to each flight. However, instrument-specific temporal drift led to small temporal discrepancies between instruments during some flights. In cases where identified plumes were misaligned in time, data were manually corrected to align the peaks where possible.

130 Data availability from some instruments for some flights was limited (see Table A1). The NO_x instrument suffered from large data gaps in three AEOG flights. This may have been because local NO_x background mole fractions were below the instrument limit-of-detection (30 pptv). However, data availability within plumes was also affected for these, and other, flights.

2.2 Flight sampling and study areas

135 This work used data collected as part of two field measurement campaigns: the Assessing Atmospheric Emissions from the Oil and Gas Industry (AEOG) programme, and the Methane Observations and Yearly Assessments (MOYA) project. The AEOG flights targeted two key production regions on the UK continental shelf (UKCS). A total of 14 flights over the North Sea in the northern UK and West Shetland region were conducted in April 2018, September 2018, or March 2019. The MOYA campaign involved three flights in July and August 2019, surveying two regions on the Norwegian continental shelf (one in the North Sea, and one in the Norwegian Sea). Figure 1 shows flight tracks for the AEOG and MOYA campaigns, as well as the offshore hydrocarbon fields and corresponding field types.

140



145 **Figure 1.** AEOG (black) and MOYA (red) flight paths in the North and Norwegian Seas. Coloured data points indicate the locations of different hydrocarbon field types (see Wilde et al., 2021b or Foulds et al., 2022 for detail). Note that the northern-most flight (~65° N) took place over the Norwegian Sea and not the North Sea. However, for the purposes of simplicity here, all sample regions are referred to as the North Sea.

2.3 Identification of flared emissions and flaring efficiency calculations

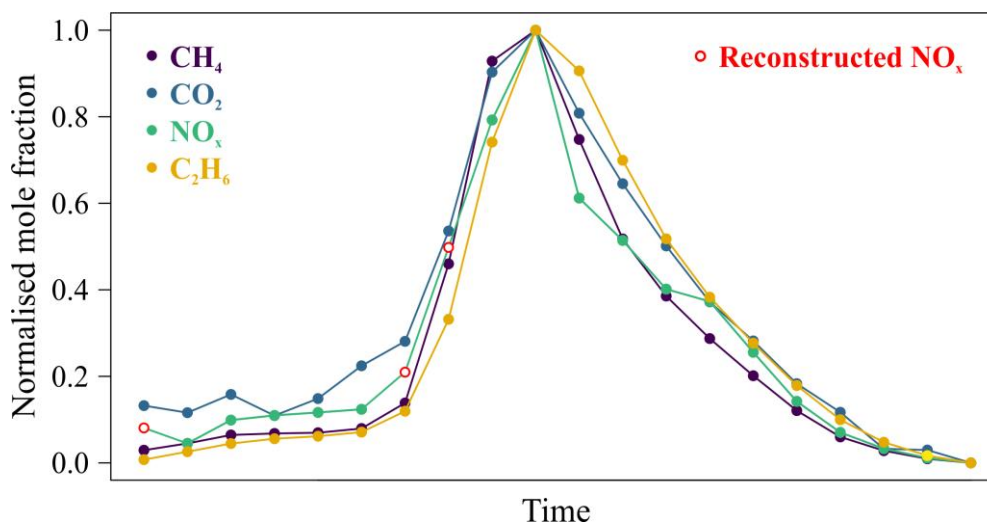
150 Gas flaring could not be confirmed visually during the flight campaigns due to distance to targeted facilities. In the absence of visual flare confirmation, plumes associated with gas flaring were identified by correlated enhancements in the expected gas-phase components of flared hydrocarbon gas (i.e. CO₂, CH₄, C₂H₆, and NO_x) above their respective background mole fractions. Plumes which did not contain correlated enhancements of all four of these components were discarded. For example, plumes containing enhancements in only CO₂, CH₄ and C₂H₆, and which therefore lacked enhancements in NO_x, were discarded as they were assumed result from gas venting without flaring. Similarly, plumes containing only enhancements in CO₂ and NO_x, and therefore lacking enhancements in either of CH₄ or C₂H₆, were assumed to result from emissions from power generation, such as diesel generators. Unfortunately, this approach does not preclude the possibility of including emissions from multiple mixed sources of CO₂, CH₄, C₂H₆, or NO_x, such as co-located venting and power generation emissions.

160 Representative median-average background CO₂, CH₄, C₂H₆ and NO_x mole fractions were determined for each plume using the 50 neighbouring 1 Hz measurements to either side of the plume. Plumes for which this was not possible due to missing background data for one or more components (i.e. fewer than 10 background data points) were discarded. Plumes were additionally discarded if one or more components lacked sufficient data within the plume (i.e. fewer than three data points). The NO_x data generally suffered from data unavailability (see Table A1), with large proportions of missing 1 Hz data.



During background measurement, missing data could be attributed largely to NO_x mixing ratios below the instrument limit-of-detection (30 pptv) but missing data within plumes was also common. If enough data were present, missing NO_x data were
165 interpolated using normalised values of the CO_2 and CH_4 plume data. Figure 2 shows an example in which three missing data points within a single plume were interpolated and reconstructed using the mean-average normalised CO_2 and CH_4 data. Using
this method relies on the assumption that each gas has an identical plume morphology, which may not always be the case if
there are multiple co-located sources upwind (France et al., 2021). However, Fig. 2 clearly demonstrates that all four gas
components showed consistent plume morphologies in this example. Finally, plumes were discarded if the maximum within-
170 plume enhancement was within two standard deviations (2σ) of the local background mole fraction.

Background mole fractions were subtracted from within-plume mole fractions to calculate enhancements. The
resultant plume enhancements were then integrated (with respect to time) to determine the amount of each component within
the emission plume. Integrating the data, rather than performing linear regression of co-located components, allows for slight
temporal discrepancies in measured plumes to be ignored. Temporal discrepancies which lead to misaligned plumes could
175 affect linear correlations between plume components.



180 **Figure 2. Normalised mole fraction (enhancements above background) for a plume containing CO_2 , CH_4 , C_2H_6 , and NO_x . Three NO_x data points were missing and were interpolated and reconstructed using the mean of normalised mole fractions of CO_2 and CH_4 (red data points).**

2.3.1 Combustion efficiency calculations

Combustion efficiency (η) can be defined in multiple ways, but is usually reported as the efficiency with which the gas flare converts hydrocarbons in the fuel gas into carbon dioxide (Equation 1; Corbin and Johnson, 2014).

$$\eta[\%] = \frac{\text{carbon in } \text{CO}_2 \text{ in flared gas}}{\text{carbon in hydrocarbon fuel gas}} \times 100 \quad (\text{Eq. 1})$$



185 However, in many cases, the amount of carbon in the industrial fuel gas is unknown. Fuel composition can vary widely between production regions and within fields, as well as over the course of production. In cases where fuel composition is not known, combustion efficiencies have previously been approximated using the relationship between enhancements of CO₂ and CH₄ measured within the flare plume (Equation 2; Nara et al., 2014).

$$\eta[\%] = \frac{\Delta CO_2}{\Delta CO_2 + \Delta CH_4} \times 100 \quad (\text{Eq. 2})$$

190 ΔCO_2 and ΔCH_4 respectively refer to the enhancement of within-plume CO₂ and CH₄ above the local background mole fractions (see Section 2.3). The method presented in Equation 2 assumes that all of the CO₂ produced during gas flaring is due to combustion of CH₄ i.e. no other hydrocarbons were combusted (the fuel gas is 100% CH₄), and that CO₂ was not initially present in the fuel gas. This can lead to a slight overestimation of combustion efficiency, if other hydrocarbons were present in the fuel gas and combusted.

195 As C₂H₆ mole fractions were also measured onboard the FAAM aircraft, additional combustion efficiencies were calculated which account for the C₂H₆ enhancement within the plumes (Equation 3). C₂H₆ oxidises to form two molar equivalents of CO₂, and is therefore accounted for twice in Eq. 3.

$$\eta[\%] = \frac{\Delta CO_2}{\Delta CO_2 + \Delta CH_4 + (2 \times \Delta C_2H_6)} \times 100 \quad (\text{Eq. 3})$$

200 Where ΔC_2H_6 refers to the enhancement of within-plume C₂H₆ above the local background mole fraction. It should be noted that combustion efficiencies calculated with Eq. 3 will still overestimate the true combustion efficiency by some amount. Although CH₄ and C₂H₆ typically dominate the fuel gas composition, other hydrocarbons are likely to be present (albeit, in small amounts) and cannot be accounted for here. However, this approach provides the best possible approximation in the absence of suitable instrumentation capable of resolving larger hydrocarbons at 1 Hz.

2.3.2 Destruction removal efficiency calculations

205 Destruction removal efficiency (DRE) is a measure of the efficiency with which a particular fuel gas component is oxidised within the flare (Equation 4; Caulton et al., 2014; Corbin and Johnson, 2014).

$$DRE_i[\%] = \left(1 - \frac{\Delta x_i}{(X_i \times \Delta CO_2) + \Delta x_i}\right) \times 100 \quad (\text{Eq. 4})$$

Where x_i refers to any component of the fuel gas, Δx_i the enhancement above background of that component within the plume, and X_i is the fractional composition of x_i in the fuel gas. Equation 4 was used to calculate DREs for CH₄ and C₂H₆.

210 Fuel gas composition values for various platforms were taken from privately communicated fuel composition data sourced via the Department for Business, Energy, and Industrial Strategy (BEIS). Where gas flare plumes could be satisfactorily attributed to single platforms (or groups of platforms), specific fuel composition values were used for X_i . In the absence of data for identified platforms, or where plumes could not be satisfactorily associated with specific platforms, the median fuel composition of all available data was used. The median fuel composition for CH₄ was 0.845, and for C₂H₆ was



215 0.085. These fuel compositional values are consistent with those used in other work (e.g. Schwietzke et al., 2014; Sherwood et al., 2017).

2.3.3 Emission ratio calculations

NO_x and C₂H₆ emission ratios (ERs) were calculated using CO₂ and CH₄ as the reference gas component.

$$ER_{NO_x} = \frac{\Delta NO_x}{\Delta CO_2} = \frac{NO_{x,plume} - NO_{x,background}}{CO_{2,plume} - CO_{2,background}} \quad (\text{Eq. 5})$$

220

$$ER_{C_2H_6} = \frac{\Delta C_2H_6}{\Delta CH_4} = \frac{C_{2H_6,plume} - C_{2H_6,background}}{CH_{4,plume} - CH_{4,background}} \quad (\text{Eq. 6})$$

ERs calculated in this way are also referred to as normalised excess mixing ratios (NEMRs), and assume that no chemical processing has occurred within the plume that could change the composition (Yokelson et al., 2013; Barker et al., 2020). This assumption is suitable for the components analysed here, as plumes were typically measured less than 10 km downwind of the source. The atmospheric lifetimes of CH₄ (~9 years; Turner et al., 2017), and C₂H₆ (~2 months; Hodnebrog et al., 2018) ensure
225 minimal chemical processing, and NO_x is a conserved quantity unaffected by the conversion of NO to NO₂ between emission and measurement.

2.4 Gas flaring emission inventories

Many emission inventories group emissions from the oil and gas sector into a single category, representing intentional venting, flaring, and leakage. The two emission inventories used here provide separate categories for flaring emissions.

230 The Global Fuel Exploitation Inventory (GFEI) is a globally gridded inventory of CH₄ emissions from oil, gas, and coal exploitation, available at 0.1° × 0.1° for 2019 (Scarpelli et al., 2020). The GFEI provides gridded emissions from different subsectors (e.g. exploration, production, transport, transmission, and refining), and from specific processes such as venting and flaring, based on country reports submitted in accordance with the United Nations Framework Convention on Climate Change (UNFCCC). CH₄ emissions from flaring during gas production, gas processing, and oil production were examined
235 here. In the GFEI, CH₄ emissions from flaring during oil exploration, gas exploration, and oil refining are grouped together with emissions from leakage and venting, and hence these emissions were not analysed. Comparisons between the GFEI and CH₄ emission fluxes measured in the North Sea have already been made by Foulds et al. (2021) and Pühl et al. (in review).

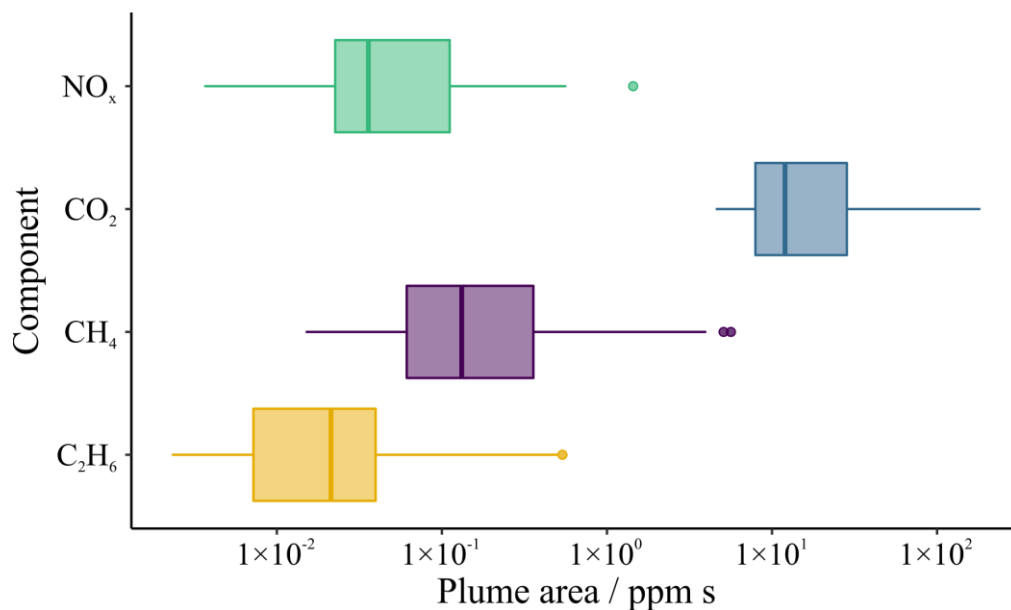
The anthropogenic emission dataset Evaluating the Climate and Air Quality Impacts of Short-lived Pollutants (ECLIPSE) v5 provides global CH₄ and NO_x emissions (amongst other pollutants) for flaring as a separate sub-sector, at 0.5°
240 × 0.5° resolution for 2020 (Stohl et al., 2015). The ECLIPSE emission dataset was created using the Greenhouse gas-Air Pollution Interactions and Synergies (GAINS) model and international and national activity data for energy usage, industrial production, and agricultural activities.



3 Results and discussion

245 Fifty-eight plumes from a maximum of 30 individual facilities were identified as containing emissions from gas flaring based on the criteria described in Section 2.3 (see Table A2 for numbers of excluded plumes). As some plumes from the same facility were sampled multiples times, there are two conceivable approaches to determining plume statistics. Firstly, measurements for plumes considered to originate from the same source could be combined, assuming that the combustion efficiency and emission ratios are constant. This would allow for uncertainty estimation, using the variability in the measured values. However, this may not be trivial as changing conditions (in e.g. wind direction) could mean that plumes do not always appear
250 in the same location and therefore cannot always be positively attributed to the exact same source (in the absence of complex and time-consuming dispersion modelling). A second approach involves treating each intercepted plume as unique, by assuming that flaring conditions vary over time and that separate plume intercepts represent distinct measurements of instantaneous emissions. In this work, it was noted that plumes considered to have the same source origin (via approximate wind direction) had similar $\Delta\text{C}_2\text{H}_6:\Delta\text{CH}_4$ emission ratios but that combustion efficiency varied with wind speed (see Appendix
255 B). Hence, we have opted to treat the 58 identified plumes as individual and unique events. The following sections therefore present combustion efficiency, destruction removal efficiencies (for CH_4 and C_2H_6) and emission ratio results for the 58 identified plumes.

Figure 3 illustrates the relative abundance of gaseous components in the 58 sampled flared plumes. As expected, CO_2 was the largest component by at least an order of magnitude. The range in CH_4 , C_2H_6 , and NO_x spanned greater than two orders
260 of magnitude. This could imply the measurement of emissions from flares of different operational characteristics and fuel gas volumes.



265 Figure 3. Box and whisker distributions of integrated plume areas (in ppm s) above background for NO_x, CO₂, CH₄, and C₂H₆ across
the 58 identified flaring plumes. Box edges correspond to the first and third quartile (i.e. the 25th and 75th percentile) with the thicker,
central line denoting the sample median (i.e. 50th percentile). The upper whisker extends to the greatest value no more than 1.5
multiples of the interquartile range (IQR) from the 75th percentile value. The lower whisker extends to the smallest value no less
270 than 1.5 multiples of the IQR from the 25th percentile. Data beyond the extents of the whiskers were considered outlying points, and
were plotted individually (as circles). Note that the x-axis has a logarithmic scale.

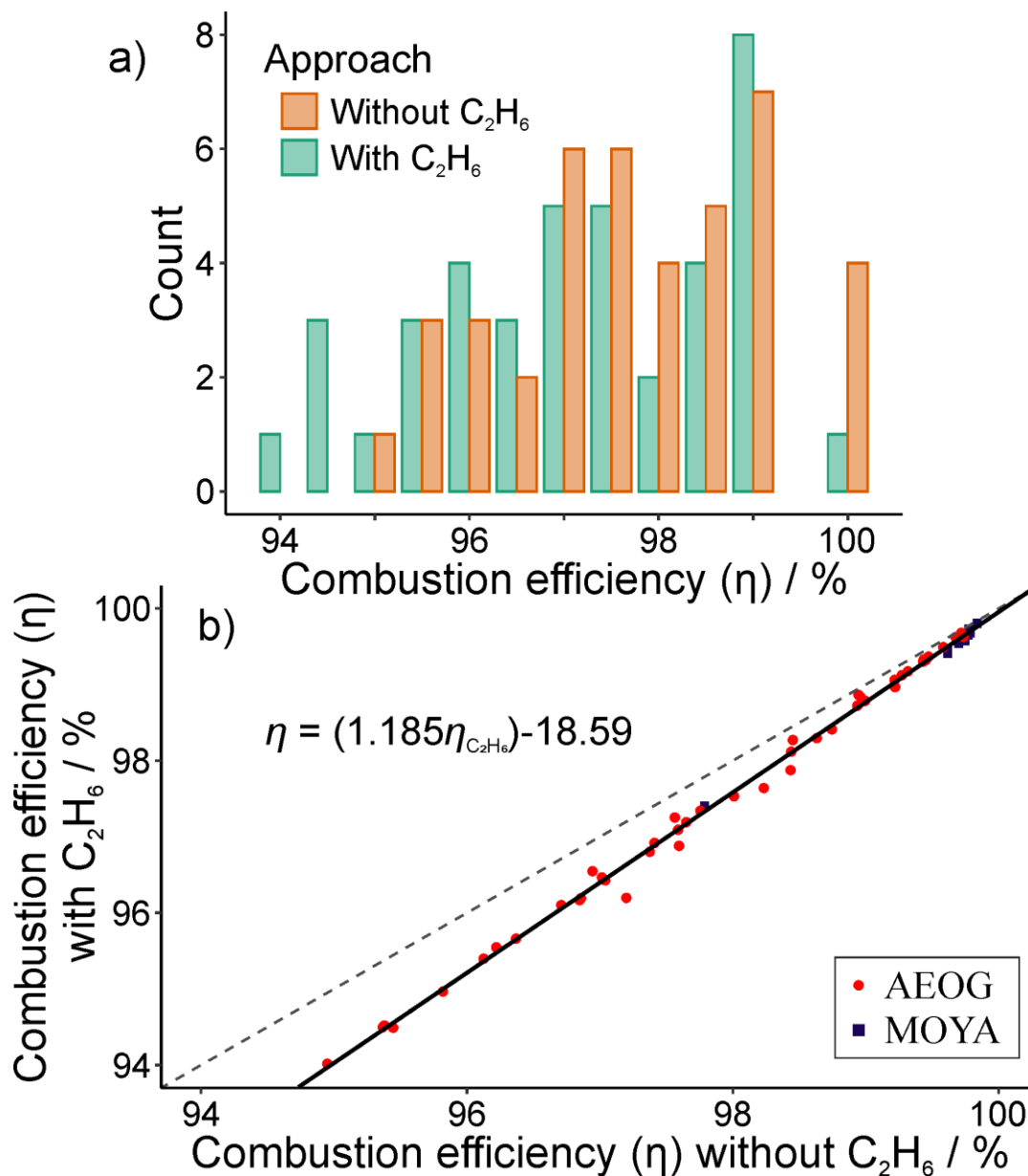


3.1 Combustion efficiency

Figure 4a shows the distribution of combustion efficiencies calculated without C_2H_6 (Eq. 2; Nara et al., 2014) and with C_2H_6 included (Eq. 3). Combustion efficiencies were marginally greater when C_2H_6 was not included in the calculation. However, even when including C_2H_6 in the calculation, efficiencies were high, with some plumes approaching 100% efficiency, and all efficiencies greater than 94%. The median combustion efficiency across all sampled plumes without C_2H_6 included was 98.7% (mean = $98.3\% \pm 1.4\%$, 1σ), and the median efficiency with C_2H_6 included was 98.4% (mean = $97.9\% \pm 1.7\%$, 1σ) (see also Fig. C1). These values are exceptionally close to the 98% combustion efficiency assumed by many emission inventories. However, Fig. 4a shows a strongly skewed distribution, indicating that assumptions of 98% combustion efficiency is likely to be an overestimate in some cases. A summary of all results can be found in Table 1.

Figure 4b shows the linear relationship between combustion efficiencies calculated with and without C_2H_6 . The linear relationship was estimated using reduced major axis regression. Combustion efficiencies calculated including C_2H_6 (Eq. 3) were marginally smaller than those calculated without C_2H_6 (Eq. 2). This relationship provides an approximation for estimating combustion efficiencies accounting for C_2H_6 in the absence of direct C_2H_6 observations. The R^2 value for the linear regression was 0.996, indicating a high degree of model fit.

There was a small difference in combustion efficiencies (calculated including C_2H_6) measured during the AEOG and MOYA campaigns. The median combustion efficiency measured during AEOG ($n = 46$ plumes) was 97.6% (mean = $97.5\% \pm 1.6\%$, 1σ) whilst the median combustion efficiency measured during MOYA ($n = 12$) was 99.6% (mean = $99.4\% \pm 0.6\%$, 1σ). We cannot provide a conclusive explanation for this small difference in combustion efficiencies between the two campaigns but propose two explanations. AEOG sampled primarily UK-based platforms whilst MOYA sampled Norwegian platforms. It may therefore be possible that differences in facility type, age, or operational practices in the two regions were responsible for the observed distinction in combustion efficiency. Alternatively, the measurements could be explained by differences in emissions from different hydrocarbon field types (see Fig. 1) with different gas compositions. Wilde et al. (2021b) measured different VOC compositions in emissions from different field types in the North Sea region, and this may align with differences in the combustion efficiency observed here. However, Plant et al. (2022) found no correlation between combustion efficiency and factors such as well age, or gas-to-oil ratio, for onshore facilities in the USA.



300 **Figure 4.** a) Histogram distribution of combustion efficiencies (η) calculated with C_2H_6 (green; Eq. 3) and without C_2H_6 (orange; Eq. 2). b) Linear relationship between combustion efficiencies calculated with C_2H_6 and without C_2H_6 . The solid black line shows the linear reduced major axis regression, with $R^2 = 0.996$. The dashed black line shows a 1:1 ratio.



Table 1. Summary of combustion efficiency, destruction removal efficiency (DRE) and emission ratio results.

Measurement (n = 58)	Median	Mean ($\pm 1\sigma$)
Combustion efficiency (without C ₂ H ₆)	98.7%	98.3% ($\pm 1.4\%$)
Combustion efficiency (with C ₂ H ₆)	98.4%	97.9% ($\pm 1.7\%$)
DRE CH ₄	98.5%	97.9% ($\pm 1.7\%$)
DRE C ₂ H ₆	97.9%	97.6% ($\pm 1.7\%$)
$\Delta\text{NO}_x:\Delta\text{CO}_2$	0.003 ppm ppm ⁻¹	0.004 (± 0.004) ppm ppm ⁻¹
	0.002 g g ^{-1*}	0.003 (± 0.003) g g ^{-1*}
$\Delta\text{NO}_x:\Delta\text{CH}_4$	0.26 ppm ppm ⁻¹	0.48 (± 0.65) ppm ppm ⁻¹
	0.63 g g ^{-1*}	1.14 (± 1.54) g g ^{-1*}
$\Delta\text{C}_2\text{H}_6:\Delta\text{CH}_4$	0.11 ppm ppm ⁻¹	0.13 (± 0.06) ppm ppm ⁻¹
	0.20 g g ⁻¹	0.24 (± 0.11) g g ⁻¹

*Assumes a NO_x molar mass of 38.01 g mol⁻¹, equivalent to 50% NO and 50% NO₂.

305

Whilst combustion efficiency is expected to decrease with increasing wind speed (Jatale et al., 2016), recent studies have found little-to-no impact on flaring efficiency at wind speeds of up to 15 m s⁻¹ (Caulton et al., 2014; Plant et al., 2022). Figure 5 shows an extremely weak but positive correlation ($p = 0.04$; $R^2 = 0.08$) between combustion efficiency and wind speed across the 58 identified plumes, although there was much scatter in the data. The observed trend was likely skewed by the greater number of plumes sampled under wind speeds of approximately 15 m s⁻¹, several of which were measured during the MOYA campaign. Plumes sampled during the MOYA campaign had typically higher combustion efficiencies and therefore may be influencing the observed trend. The only plume measured in wind speeds of approximately 20 m s⁻¹ (19.6 m s⁻¹) showed a lower combustion efficiency (~95.0%) relative to many of those measured at wind speeds of 15 m s⁻¹. Unfortunately, this was an isolated measurement and a larger sample size of plumes sampled under higher wind speeds (> 15 m s⁻¹) would be required to draw meaningful conclusions on combustion efficiencies at such wind speeds. Our results were therefore in agreement with the conclusions of both Caulton et al. (2014) and Plant et al. (2022), which both showed no statistical relationship between combustion efficiency and wind speed.

320

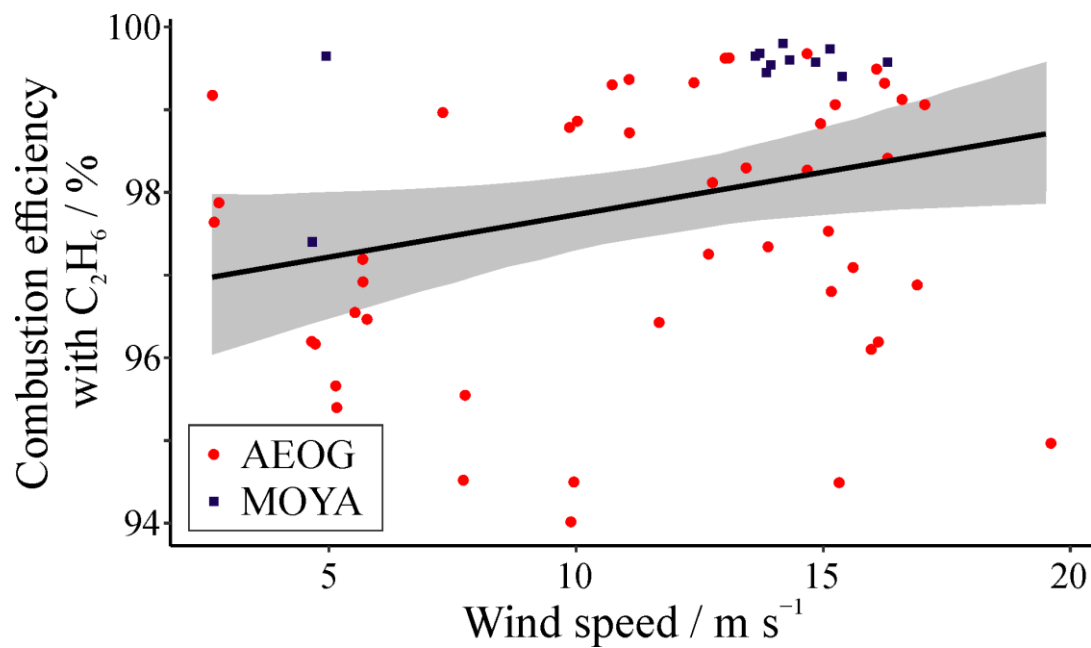
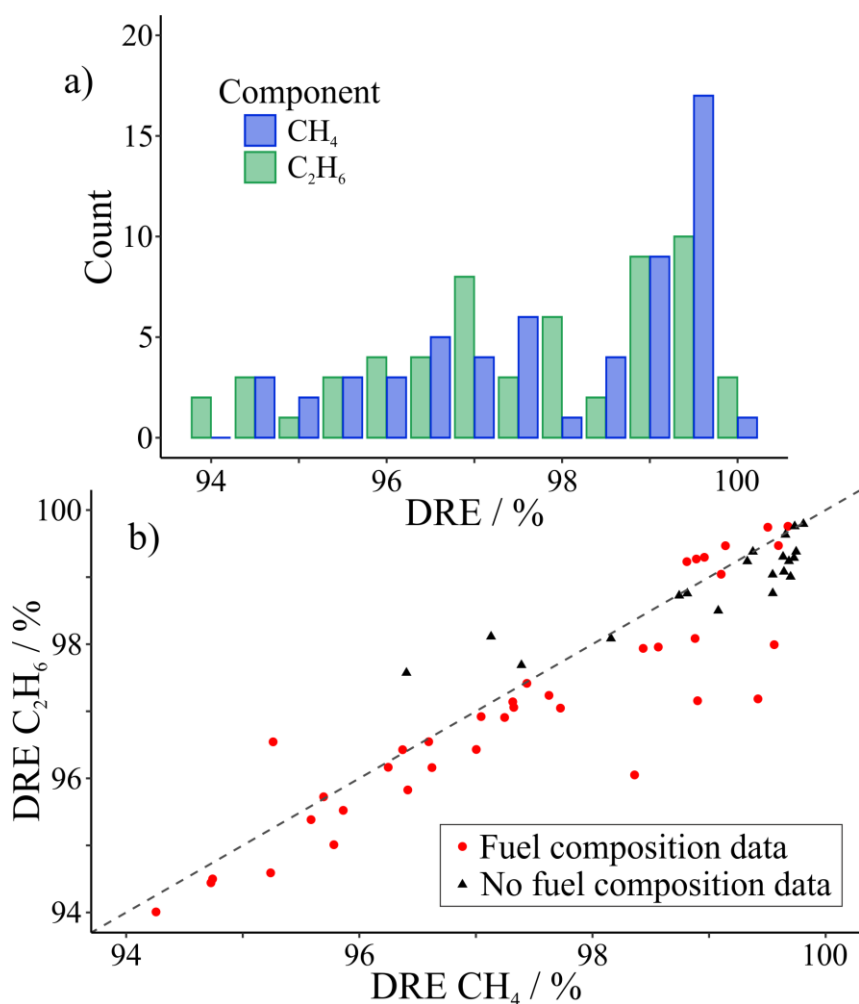


Figure 5. Correlation between combustion efficiency (calculated including C_2H_6 ; Eq. 3) and wind speed ($m s^{-1}$). The wind speed for each plume was calculated as the mean of 1 Hz wind speeds measured during, and both 50 seconds before and after the plume. The black line shows an ordinary least squares linear regression of the data ($p = 0.04$, $R^2 = 0.08$), with the 95% confidence interval shown in grey.

325

3.2 Destruction removal efficiencies (DREs)

Figure 6a shows the distribution of DREs calculated for both CH_4 and C_2H_6 using Eq. 4 and fuel composition data provided by BEIS. The efficiency of CH_4 destruction was marginally greater than that for C_2H_6 , with median values of 98.5% (mean = 97.9% \pm 1.7%, 1σ) and 97.9% (mean = 97.6% \pm 1.7%, 1σ) for CH_4 and C_2H_6 respectively (Table 1; see also Fig. C2). Gvakharia et al. (2017) reported marginally lower median DRE values of 97.1% (\pm 0.4%) for CH_4 , and of 97.3% (\pm 0.3%) for C_2H_6 , from 37 flare plumes in the Bakken formation, United States. Plant et al. (2022) reported mean DRE values for CH_4 of 97.3%, 96.5%, and 91.7% from the Eagle Ford, Bakken, and Permian basins (United States) respectively. These results are in excellent agreement with our own. Figure 6b shows the relationship between DREs for the two fuel components, with a strong correlation between the two, even for DREs calculated for plumes from platforms for which flare gas composition was not available (see Section 2.3.2).





340 **Figure 6. a) Histogram distribution of destruction removal efficiencies (DREs) calculated for CH₄ (blue) and for C₂H₆ (green). b) Comparison of DREs for CH₄ and C₂H₆. The black dashed line shows a 1:1 ratio. The median fuel composition (CH₄ = 0.845, C₂H₆ = 0.085) was used for plumes emitted from platforms for which no fuel composition data were available (black triangles).**

3.3 Emission ratios

Figure 7 shows the distribution of NO_x emission ratios calculated using both CO₂ and CH₄ as reference gases ($\Delta\text{NO}_x:\Delta\text{CO}_2$ and $\Delta\text{NO}_x:\Delta\text{CH}_4$ respectively). Mean NO_x emission ratios were 0.004 ± 0.004 (1 σ ; median = 0.003) ppm ppm⁻¹ when using
345 CO₂ as the reference gas, and 0.48 ± 0.65 (1 σ ; median = 0.26) ppm ppm⁻¹ when using CH₄ as the reference gas (Table 1). There was substantial variability in the amount of NO_x produced relative to both CO₂ and CH₄, as indicated by the large standard deviations about the mean ratios and the skewed long-tail distributions in both Fig. 7a and 7b. This may be a consequence of the inclusion of mixed emission sources within our dataset; it is difficult to distinguish between plumes containing pure flaring emissions, and those potentially containing mixed emissions from co-located sources.

350 Four of the five greatest $\Delta\text{NO}_x:\Delta\text{CH}_4$ ratios (>1.1 ppm ppm⁻¹) were measured over deep-water oilfields west of the Shetland Isles, where oil production is typically performed by Floating Production Storage and Offloading (FPSO) vessels. An additional high $\Delta\text{NO}_x:\Delta\text{CH}_4$ ratio (of 1.5 ppm ppm⁻¹) was measured in a shallow water field, east of Scotland, also operated by an FPSO. FPSO vessels have been reported to contribute to 21% of all offshore flaring volume (Charles and Davis, 2021), and the high $\Delta\text{NO}_x:\Delta\text{CH}_4$ ratios measured in the vicinity of their operation here could indicate a difference in operational
355 practice (e.g. diesel generators onboard FPSO vessels contributing to NO_x emissions) compared with fixed platforms. The same five FPSO plumes also had the five greatest $\Delta\text{NO}_x:\Delta\text{CO}_2$ ratios.

Typically, NO_x emissions from flares are estimated using emission factors and activity rates, and often use flare heat as a proxy for NO_x emission rates. Torres et al. (2012c) reported a mean NO_x:CO₂ ratio of 0.00020 (± 0.00014) ppb ppb⁻¹ from
360 24 test flares operated under a range of conditions (fuel gas composition, fuel gas flow, lower heating value, and steam or air assisted flow). In comparison, the smallest $\Delta\text{NO}_x:\Delta\text{CO}_2$ ratio measured in this study was 0.0005 ppb ppb⁻¹.

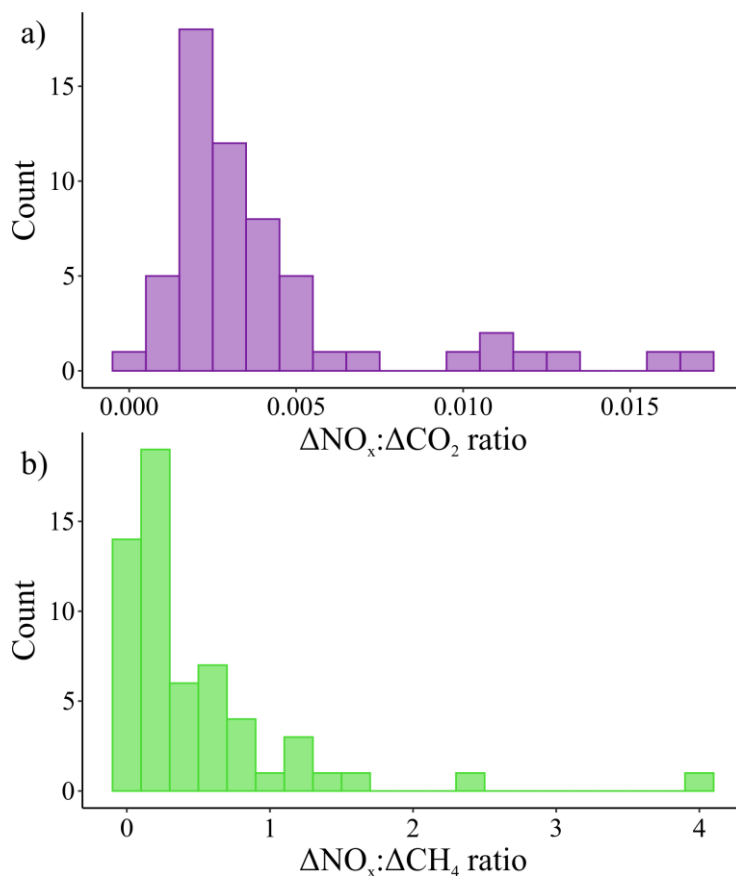
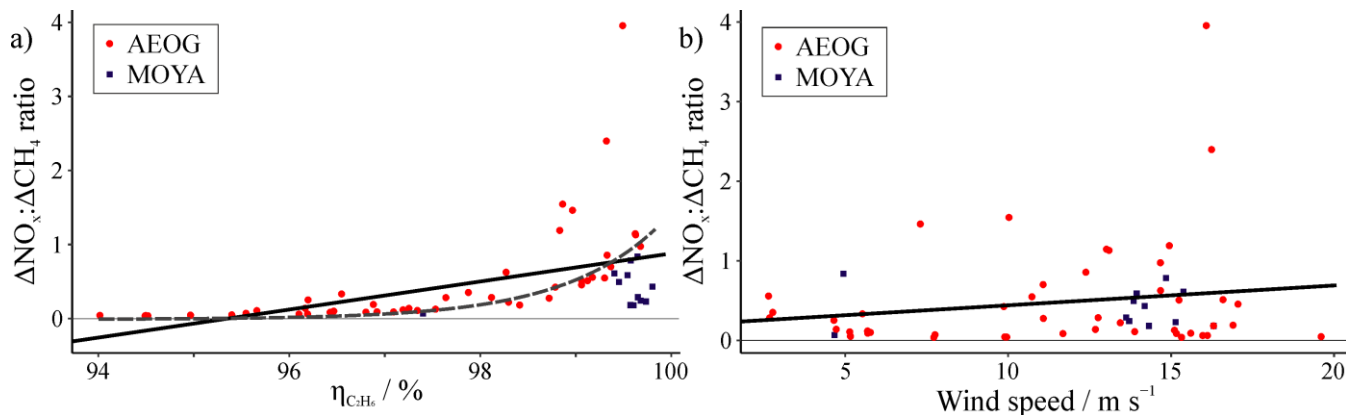


Figure 7. Histogram distribution of NO_x emission ratios (ppm ppm⁻¹) a) calculated using CO₂ as the reference gas; and b) calculated using CH₄ as the reference gas.

365

Figure 8a shows the relationships between combustion efficiency (calculated with C₂H₆) and $\Delta\text{NO}_x:\Delta\text{CH}_4$. Higher combustion efficiencies were typically associated with higher relative amounts of NO_x, consistent with higher temperature flaring. Figure 8a appears to show an exponential relationship between combustion efficiency and $\Delta\text{NO}_x:\Delta\text{CH}_4$, but a linear regression is also shown for comparison ($p = 9.3 \times 10^{-5}$; $R^2 = 0.24$). NO_x only appeared to be produced in substantial amounts (relative to CH₄) at combustion efficiencies greater than ~96%, with a general increase in NO_x ratios with increasing combustion efficiency beyond this point. However, plumes measured during the MOYA campaign appeared to have reduced NO_x ratios relative to many of those measured in AEOG, despite having greater combustion efficiencies, implying possible differences in flare operation. Torres et al. (2012c) found a similar result, with minimal NO_x produced below a combustion efficiency threshold of roughly 80%, above which NO_x production increased roughly linearly. Wind speed appeared to have very little influence on NO_x emission ratios ($p = 0.2$; $R^2 = 0.03$) (Fig. 8b).

370
375



380 **Figure 8. Correlation between measured $\Delta\text{NO}_x:\Delta\text{CH}_4$ ratio and a) combustion efficiency calculated with C_2H_6 ($\eta_{\text{C}_2\text{H}_6}$), and; b) wind speed. Solid black lines show ordinary least squares linear regressions with $p = 9.3 \times 10^{-5}$ and 0.2, and $R^2 = 0.24$ and 0.03, for the relationship with combustion efficiency and wind speed respectively. Dashed black line shows the exponential relationship ($y = e^x$) between $\Delta\text{NO}_x:\Delta\text{CH}_4$ and combustion efficiency, for comparison.**

385 The mean $\Delta\text{C}_2\text{H}_6:\Delta\text{CH}_4$ ratio across all gas flaring plumes was 0.13 ± 0.06 (1σ) ppm ppm^{-1} , with ratios ranging between 0.04 and 0.33 (median = 0.11) ppm ppm^{-1} (Table 1; Fig. C3). These results were in excellent agreement with measurements reported by Wilde et al. (2021b), in which $\Delta\text{C}_2\text{H}_6:\Delta\text{CH}_4$ ratios ranged between 0.03 and 0.18 ppm ppm^{-1} . Ratios of between 0.03 and 0.08 ppm ppm^{-1} were also measured for oil and gas emissions in the southern North Sea (Pühl et al., in review). $\Delta\text{C}_2\text{H}_6:\Delta\text{CH}_4$ ratios greater than 0.1 ppm ppm^{-1} are typically associated with emissions from oil wells, whilst ratios below 0.1 ppm ppm^{-1} are usually associated with emissions from gas wells (Xiao et al., 2008; Wilde et al., 2021a).

390



3.4 Emission inventories

The ECLIPSE inventory contains flaring emission products for both CH_4 and NO_x , and hence the $\text{NO}_x:\text{CH}_4$ ratio for this dataset was calculated. Figure 9 shows the ECLIPSE $\text{NO}_x:\text{CH}_4$ emission ratio in the North Sea, in units of mass per unit mass. Conversion of the $\Delta\text{NO}_x:\Delta\text{CH}_4$ ratio measured in this work (in units of mole fraction per unit mole fraction) yields a median $\Delta\text{NO}_x:\Delta\text{CH}_4$ of 0.63 g g^{-1} (mean = $1.14 (\pm 1.54) \text{ g g}^{-1}$). The measured values were roughly 30 times greater than the highest ECLIPSE ratios in the North Sea, although $\text{NO}_x:\text{CH}_4$ ratios in the ECLIPSE inventory globally reached values greater than 2.0 Gg Gg^{-1} (see Appendix D). Our study finds that the ECLIPSE inventory may underestimate the $\text{NO}_x:\text{CH}_4$ ratio by more than an order of magnitude in the North Sea region.

400

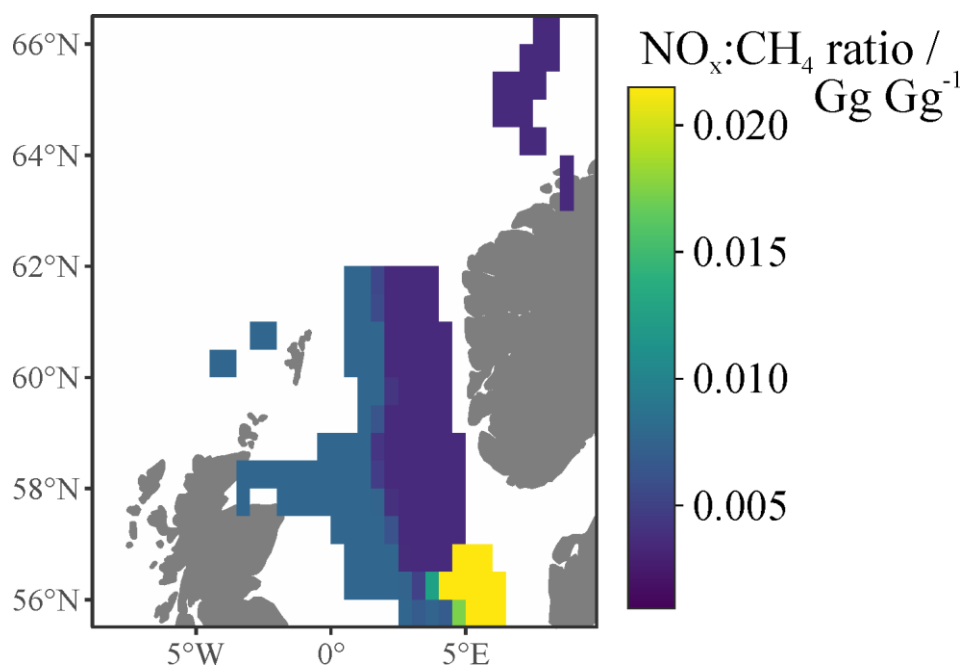


Figure 9. ECLIPSE v5 $\text{NO}_x:\text{CH}_4$ ratios in the North Sea.



4 Atmospheric implications

405 Flaring in the UK North Sea reportedly fell by 19% in 2021, but 740 million cubic metres ($7.4 \times 10^8 \text{ m}^3$) of natural gas were still reported to have been flared (OGA, 2021). Here, we use the median gas composition of flared gas provided by BEIS for this region ($\text{CH}_4 = 0.845$, and $\text{C}_2\text{H}_6 = 0.085$), and the median DREs for CH_4 and C_2H_6 (calculated in Section 3.2) to estimate total emissions of CO_2 , CH_4 , and C_2H_6 from North Sea flaring. We estimate that flaring in the UK North Sea resulted in total emissions of $1.4 \text{ Tg yr}^{-1} \text{ CO}_2$, $6.3 \text{ Gg yr}^{-1} \text{ CH}_4$, and $1.7 \text{ Gg yr}^{-1} \text{ C}_2\text{H}_6$. Using the calculated CH_4 emission total here, and the

410 median $\Delta\text{NO}_x:\Delta\text{CH}_4$ ratio derived in Section 3.3, we estimate total emissions of $3.9 \text{ Gg yr}^{-1} \text{ NO}_x$ from flaring in the North Sea region. These values, estimated using reported flaring volumes and statistics measured as part of this work, can be compared against the total emissions estimated by inventories for the North Sea region. ECLIPSE reports 30 times greater emissions of CH_4 from the North Sea, with $177 \text{ Gg yr}^{-1} \text{ CH}_4$, but smaller emissions of NO_x of $0.9 \text{ Gg yr}^{-1} \text{ NO}_x$. The lower NO_x estimate is potentially the result of the lower $\text{NO}_x:\text{CH}_4$ ratio in the ECLIPSE model, which largely underestimated the $\text{NO}_x:\text{CH}_4$ ratio

415 relative to that measured in this work (Section 3.4). Alternatively, the Global Fuel Exploitation Inventory (GFEI) provides CH_4 emissions of $13.9 \text{ Gg yr}^{-1} \text{ CH}_4$, 3 times greater than our own estimate here for the North Sea region. The GFEI total can be broken down into $11.8 \text{ Gg yr}^{-1} \text{ CH}_4$ (85%) from flaring during oil exploitation, $1.5 \text{ Gg yr}^{-1} \text{ CH}_4$ (11%) from gas processing, and $0.5 \text{ Gg yr}^{-1} \text{ CH}_4$ (4%) from gas production. Neither inventory provided flaring emission products for CO_2 or C_2H_6 , and GFEI did not include NO_x flaring emissions. These results are summarised in Table 2.

420

Table 2. Estimated total emissions of CO_2 , CH_4 , C_2H_6 , and NO_x from flared natural gas in the North Sea (in Gg), and globally (in Tg).

Data source	North Sea Flaring Emissions / Gg yr ⁻¹				Global Flaring Emissions* / Tg yr ⁻¹			
	CO ₂	CH ₄	C ₂ H ₆	NO _x	CO ₂	CH ₄	C ₂ H ₆	NO _x
This work	1400	6.3	1.7	3.9	245	5.6	1.1	3.6
ECLIPSE ¹		177		0.9		109		0.3
GFEI ²		13.9				0.6		
IEA ³					265	8		
Plant et al. (2022)						7.6		

* Uses the DRE measured in this work for offshore flaring (25% of global total; IEA, 2018), and the DRE measured by Plant et al. (2022) for onshore flaring (75% of global total; IEA, 2018). ¹ Stohl et al., 2015. ² Scarpelli et al., 2020. ³ IEA, 2021.

425

Extrapolating the results of this work to the global scale relies on the crude assumption that global natural gas supplies are analogous to those found in the North Sea, and that operational practices are consistent across all fields and regions both onshore and offshore. Such an extrapolation could be useful even with these substantial assumptions, as measurements of



combustion efficiencies and NO_x emission ratios from flared gas are exceptionally rare, especially offshore. Plant et al. (2022) presented a global extrapolation of their own measured flaring efficiency, estimating global total emissions of 7.6 Tg CH_4 using an effective DRE_{CH_4} (which includes measures of unlit flares) of 91.1%. The proportion of unlit flares was observed to be between 3% and 5% of all flares across different onshore basins in the United States (Lyon et al., 2021; Plant et al., 2022) and therefore may be significant for extrapolating total emissions. If we assume the DRE_{CH_4} value measured by Plant et al. (2022) is appropriate for all onshore production, and that our own measured DRE values are appropriate for offshore production, we can provide an alternative global extrapolation that accounts for any systematic differences between onshore and offshore flaring.

Approximately 25% of global oil and gas supplies are produced offshore (IEA, 2018). The IEA reported that 142 billion cubic metres ($142 \times 10^9 \text{ m}^3$) of natural gas were flared worldwide in 2020 (IEA, 2021). If flaring is practiced to the same extent both onshore and offshore, then it follows that offshore flaring was responsible for approximately $36 \times 10^9 \text{ m}^3$ of the global total. By assuming that the median DREs calculated here and the median fuel gas composition values provided by BEIS for North Sea platforms are appropriate for offshore production globally, we estimate global offshore flaring emissions of 65 Tg yr^{-1} CO_2 , 0.3 Tg yr^{-1} CH_4 , and 0.08 Tg yr^{-1} C_2H_6 . Using the onshore measured effective DRE for CH_4 from Plant et al. (2022) for both CH_4 and C_2H_6 , we estimate global onshore flaring emissions of 180 Tg yr^{-1} CO_2 , 5.3 Tg yr^{-1} CH_4 , and 1.0 Tg yr^{-1} C_2H_6 . Total global emissions, from both onshore and offshore flaring, were therefore 245 Tg yr^{-1} CO_2 , 5.6 Tg yr^{-1} CH_4 , and 1.1 Tg yr^{-1} C_2H_6 . Our estimate of CO_2 emissions is consistent with the IEA estimate, but our estimate of CH_4 emission is lower. This is due to the higher combustion efficiency measured for the North Sea (median = 98.4%) and used for offshore estimates, compared to the lower estimate of 92% used by the IEA for both onshore and offshore flaring globally. Using the median $\Delta\text{NO}_x:\Delta\text{CH}_4$ ratio, flaring was estimated to be responsible for emissions of 3.6 Tg yr^{-1} NO_x globally. Comparing to the emission inventories, ECLIPSE provides much greater total annual emissions of CH_4 , of 109 Tg yr^{-1} , but lower emissions of NO_x , of 236 Gg yr^{-1} . GFEI provides total global CH_4 emissions of 630 Gg yr^{-1} , of which oil exploitation contributes 500 Gg yr^{-1} (79%), gas processing 95 Gg yr^{-1} (15%), and gas production 35 Gg yr^{-1} (6%). Total global emissions of CO_2 , CH_4 , C_2H_6 , and NO_x are summarised in Table 2.

5 Conclusions

Fifty-eight plumes were identified as containing emissions likely to result from flaring of natural gas from offshore oil and gas facilities in the North Sea. Combustion efficiency, the efficiency with which the flares convert carbon in the fuel gas into CO_2 , was calculated for each of these plumes using two approaches; with and without accounting for C_2H_6 in the flare plume. The median combustion efficiency, of 98.4% (with C_2H_6) and 98.7% (without C_2H_6), was in agreement with the assumed value of 98% used by many emission inventories for flaring combustion efficiency. The linear relationship between combustion efficiencies calculated with and without C_2H_6 could be used to derive more accurate combustion efficiencies in the absence of measurements of C_2H_6 , assuming similar fuel gas composition. Destruction removal efficiencies (DREs) were also calculated



for CH₄ and C₂H₆ in each plume, making use of fuel gas compositions provided by BEIS. Median DRE values were 98.5% and 97.9% for CH₄ and C₂H₆ respectively.

NO_x emission ratios were calculated using both CO₂ and CH₄ as reference gases, with median values of 0.003 and 0.26 ppm ppm⁻¹ for CO₂ and CH₄ as a reference respectively. All five of the greatest ΔNO_x:ΔCH₄ ratios (>1.1 ppm ppm⁻¹) and
465 ΔNO_x:ΔCO₂ ratios (>0.011 ppm ppm⁻¹) were measured in the vicinity of Floating Production Storage and Offloading vessels, which may indicate a difference in their flaring operation compared with fixed platforms. C₂H₆ emission ratios were calculated using CH₄ as a reference gas. The median value for ΔC₂H₆:ΔCH₄, of 0.11, was in excellent agreement with C₂H₆ emission ratios calculated for similar datasets. Wind speed appeared to have only a small impact on both the combustion efficiency of the flares, and the relative amount of NO_x produced, although more data on flares operating in wind speeds of greater than 15
470 m s⁻¹ are needed.

Total North Sea and total global emissions due to flaring were estimated using reported gas flaring volumes and the statistics calculated in this work. For the North Sea, emissions were estimated as 1.4 Tg yr⁻¹ CO₂, 6.3 Gg yr⁻¹ CH₄, 1.7 Gg yr⁻¹ C₂H₆, and 3.9 Gg yr⁻¹ NO_x, whilst globally emissions were extrapolated to 245 Tg yr⁻¹ CO₂, 5.6 Tg yr⁻¹ CH₄, 1.1 Tg yr⁻¹ C₂H₆, and 3.6 Tg yr⁻¹ NO_x. Although many emission inventories do include emissions from flaring, most do not provide separate
475 values for this source, and instead aggregate emissions due to flaring with other oil and gas sector emissions. This makes comparison challenging. However, we find that the ECLIPSE inventory overestimates CH₄ emissions from flaring by a factor of 30 in the North Sea, but underestimates NO_x emissions by a factor of 4. The GFEI product overestimates CH₄ emissions from flaring by a factor of 2 in the North Sea.

The skewed distribution of combustion efficiencies found in this, and other, studies indicates that many flares operate
480 below the assumed standard efficiency for combustion. Inefficient combustion, together with the prevalence of unlit flares which directly vent CH₄ to atmosphere, contribute to large CH₄ emissions. Hence, improving natural gas disposal and flaring practices represents a viable strategy for mitigating carbon emissions from the oil and gas sector.



Appendix A: Impact of data availability on plume exclusions

485

Table A1. Data availability (percentage of total 1 Hz data) for CO₂, CH₄, C₂H₆, and NO_x during FAAM AEOG and MOYA flights. Data availability below 50% are highlighted in red. It should be noted that 100% data availability would not be expected for various reasons. Firstly, data files might contain data outside of when the instruments were operational (e.g. before take-off, or after landing) which were removed for analysis; and secondly, due to the presence of instrument calibrations, for which data were flagged and removed.

490

Flight No.	CO ₂ data / %	CH ₄ data / %	C ₂ H ₆ data / %	NO _x data / %
C099	87	87	53	56
C100	83	83	39	18
C102	88	88	53	53
C118	83	83	31	3.0
C119	83	83	50	40
C120	86	86	17	6.0
C121	84	84	29	50
C147	92	92	13	20
C148	94	94	50	2.7
C149	93	93	17	39
C150	95	95	32	3.5
C151	95	95	23	22
C191	89	89	72	58
C193	90	90	74	25

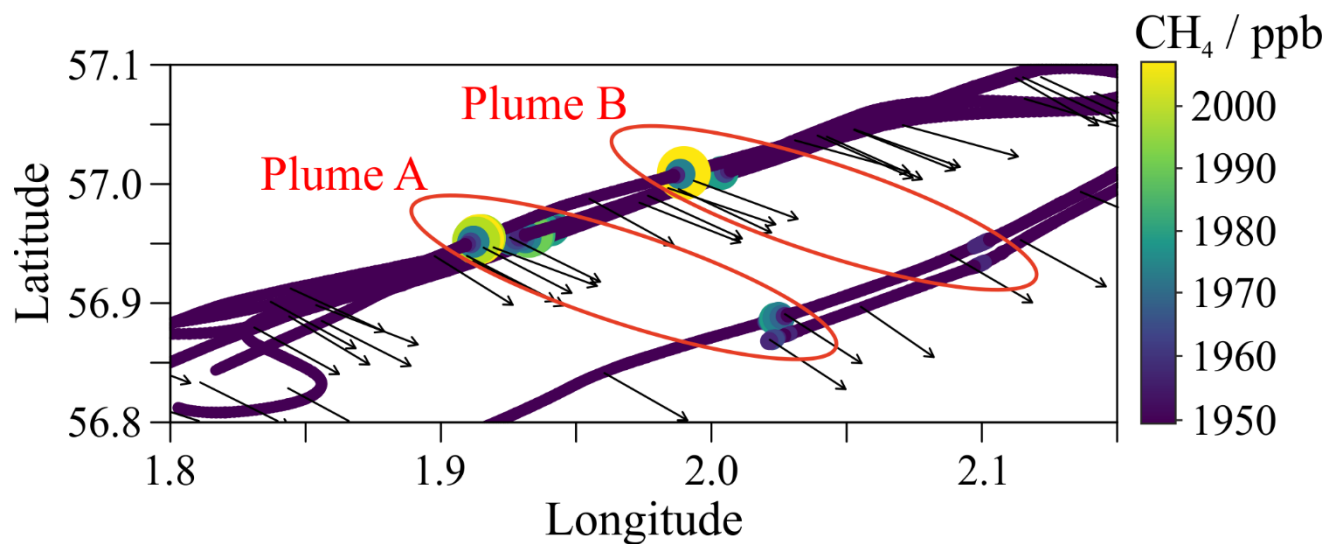


495 **Table A2. Reasons for plume exclusion. See Section 2.3 for detailed criteria descriptions. Note that plumes could be excluded based on failing multiple criteria.**

Component	Background values < 10	Within-plume values < 3	Low maximum enhancement < 2σ above background
CH ₄	0	0	0
CO ₂	0	0	1
NO _x	44	11	2
C ₂ H ₆	4	9	7



Appendix B: Comparing results for plumes with the same source origin



500 **Figure B1.** CH₄ mole fraction (see colour scale) measurements in the North Sea on 4 March 2019. Black arrows show the 60 second mean wind direction. Two distinct emission plumes (containing enhancements in CH₄ as well as CO₂, NO_x, and C₂H₆) are shown, labelled Plume A and Plume B. Note that some of these peaks were removed from analysis due to a lack of measured data (primarily NO_x) either within plume or within the background (see Appendix A).

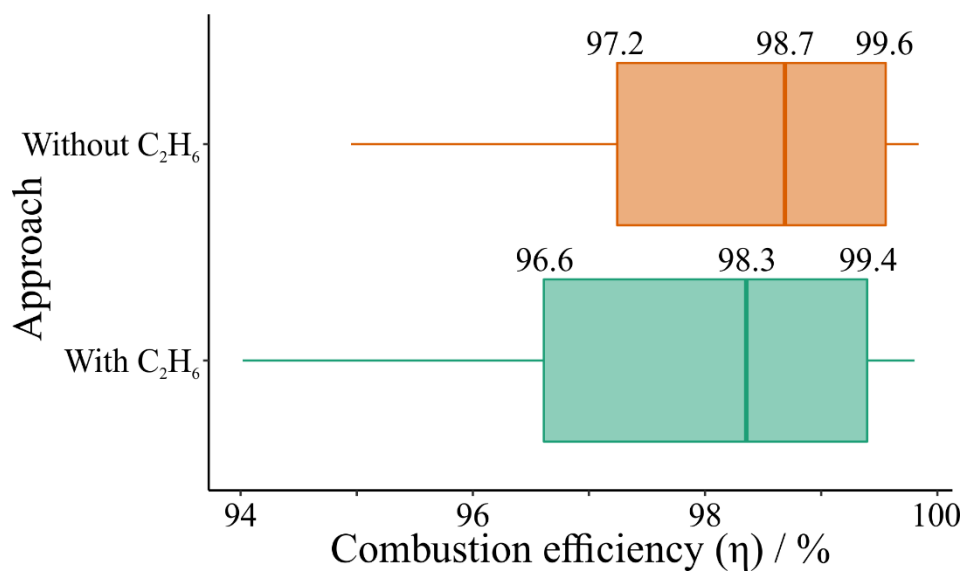


505 **Table B1. Combustion efficiencies (with and without C₂H₆) and emission ratios for peaks within two plumes sampled on 4 March 2019 (see Fig. B1).**

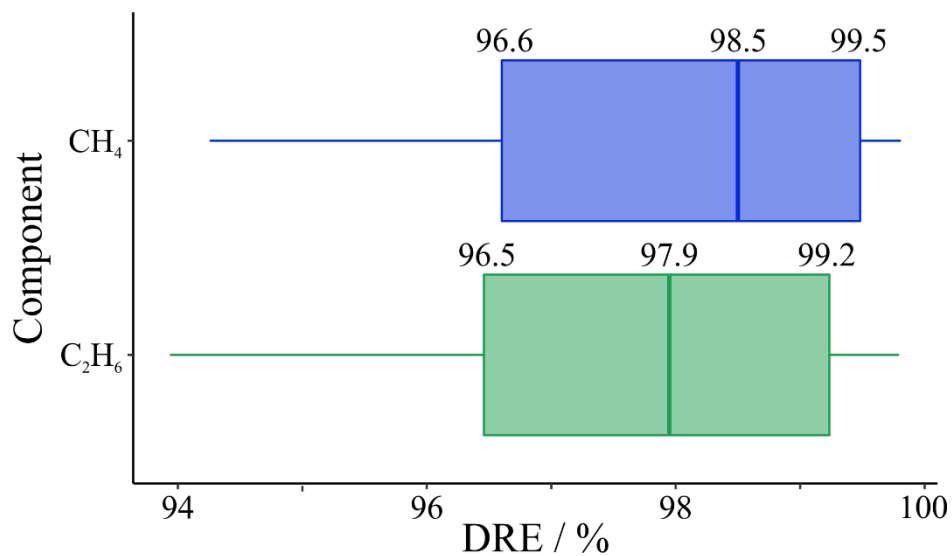
Plume 1								
Time	Latitude	Longitude	Wind speed / m s ⁻¹	Combustion efficiency (without C ₂ H ₆)	Combustion efficiency (with C ₂ H ₆)	NO _x :CO ₂	NO _x :CH ₄	C ₂ H ₆ :CH ₄
14:07	56.96	1.94	15.3	95.4	94.5	0.0018	0.038	0.111
14:14	56.96	1.94	19.6	95.8	95.0	0.0021	0.047	0.107
14:19	56.95	1.93	15.2	97.4	96.8	0.0024	0.087	0.113
14:26	56.96	1.93	16.1	96.9	96.2	0.0020	0.062	0.110
14:33	56.96	1.92	15.6	97.6	97.1	0.0022	0.090	0.106
Average			16.4 ± 1.8	96.6 ± 0.9	95.9 ± 1.1	0.0021 ± 0.0002	0.065 ± 0.023	0.109 ± 0.003
Plume 2								
14:08	57.01	2.00	13.9	97.8	97.3	0.0025	0.11	0.095
14:13	57.01	2.00	17.1	99.2	99.1	0.0036	0.46	0.100
14:21	57.01	2.00	13.4	98.6	98.3	0.0031	0.22	0.124
14:34	57.01	2.00	15.1	98.0	97.5	0.0026	0.13	0.123
14:52	56.95	2.10	16.3	98.7	98.4	0.0023	0.18	0.134
Average			15.2 ± 1.5	98.5 ± 0.6	98.1 ± 0.7	0.0028 ± 0.0005	0.22 ± 0.14	0.115 ± 0.017



Appendix C: Additional data presentation



510 **Figure C1.** Box and whisker plots of combustion efficiencies calculated without C₂H₆ (Eq. 2; orange, top row) and with C₂H₆ (Eq. 3; green, bottom row).



515 **Figure C2.** Box and whisker plots of destruction removal efficiencies (DREs) for CH₄ (blue; top row) and C₂H₆ (green; bottom row).

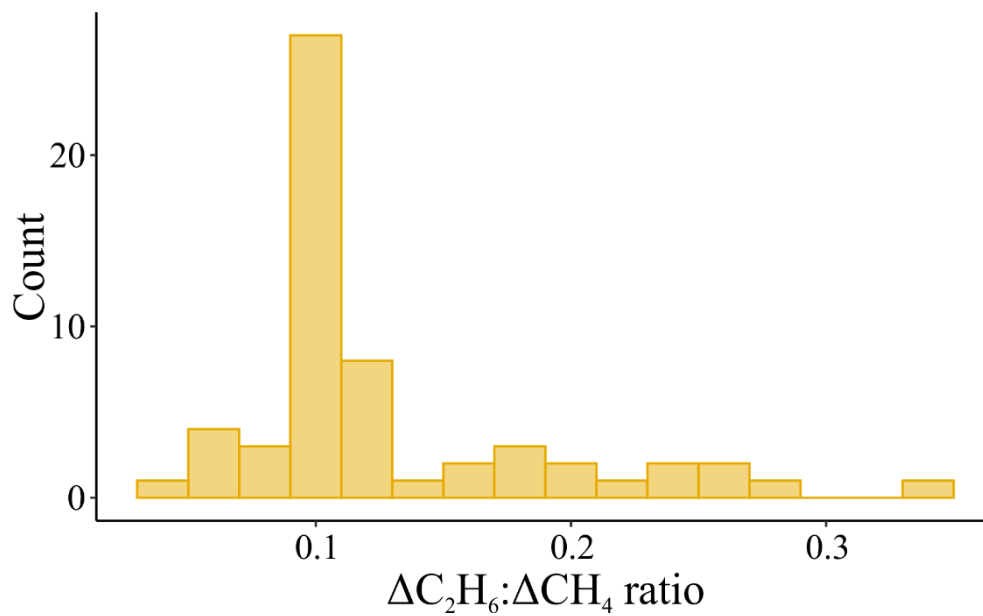
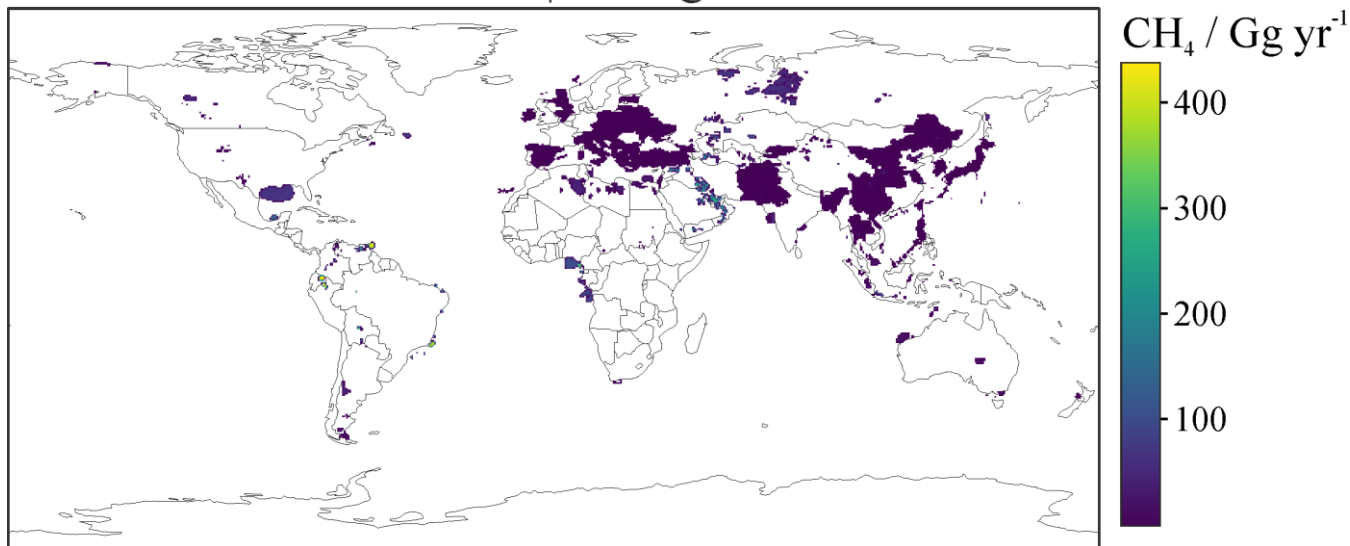


Figure C3. Histogram distribution of $\Delta C_2H_6:\Delta CH_4$ ratios.



Appendix D: Flaring emissions inventory maps (global and North Sea)

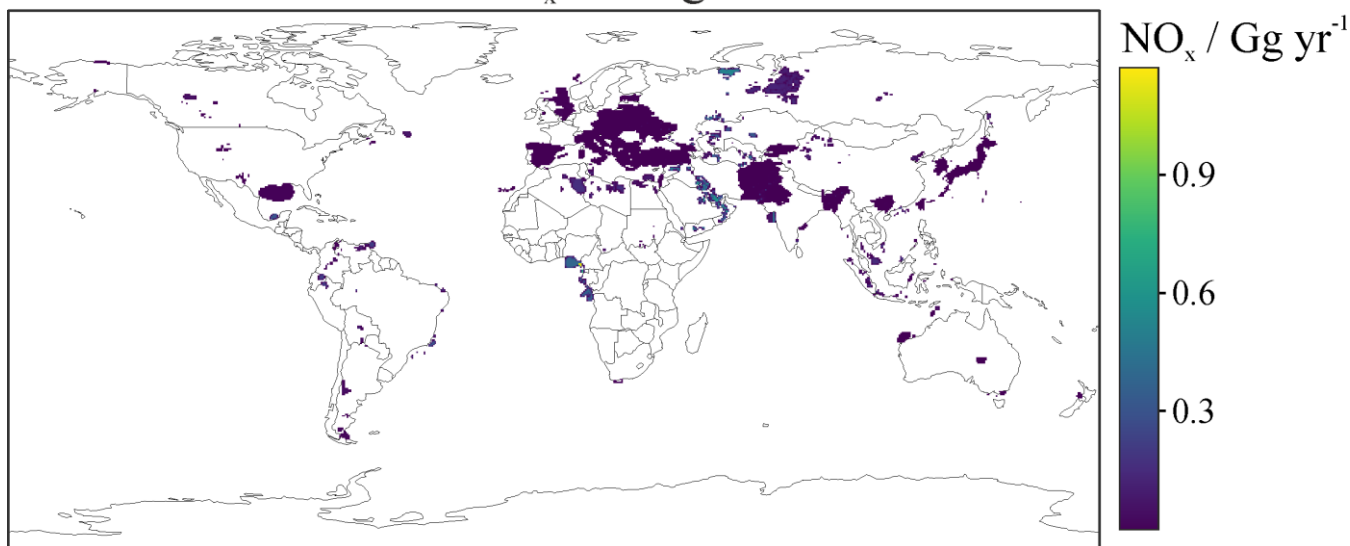
ECLIPSE v5 CH₄ flaring emissions



520

Figure D1. ECLIPSE v5 global CH₄ flaring emissions at 0.5° × 0.5° for 2020 (Stohl et al., 2015).

ECLIPSE v5 NO_x flaring emissions



525

Figure D2. ECLIPSE v5 global NO_x flaring emissions at 0.5° × 0.5° for 2020 (Stohl et al., 2015).



GFEI CH₄ flaring emissions

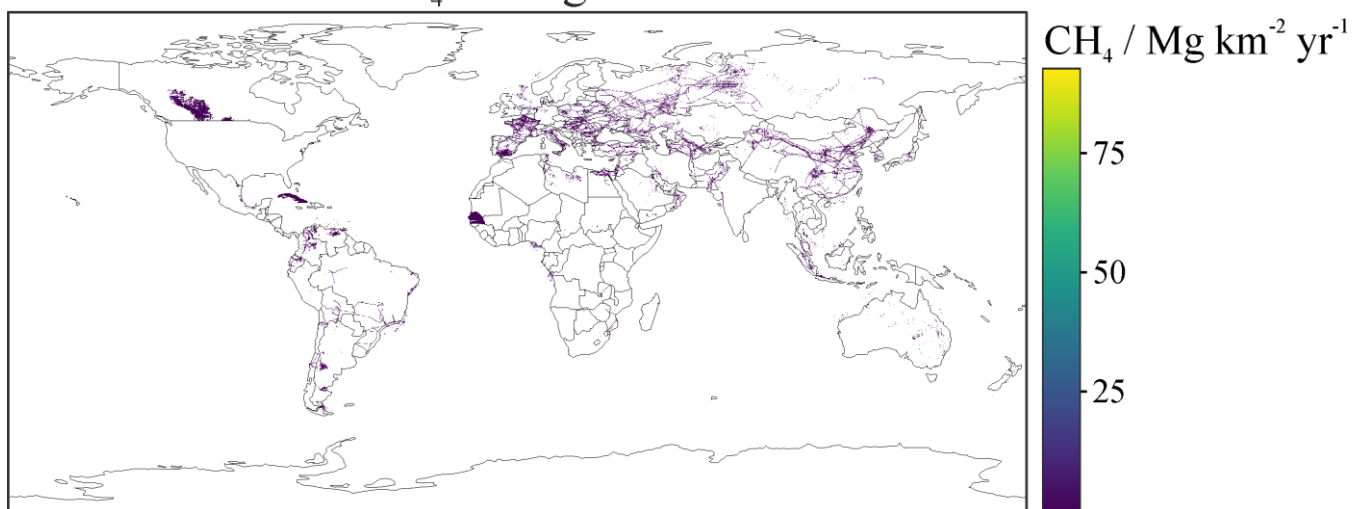
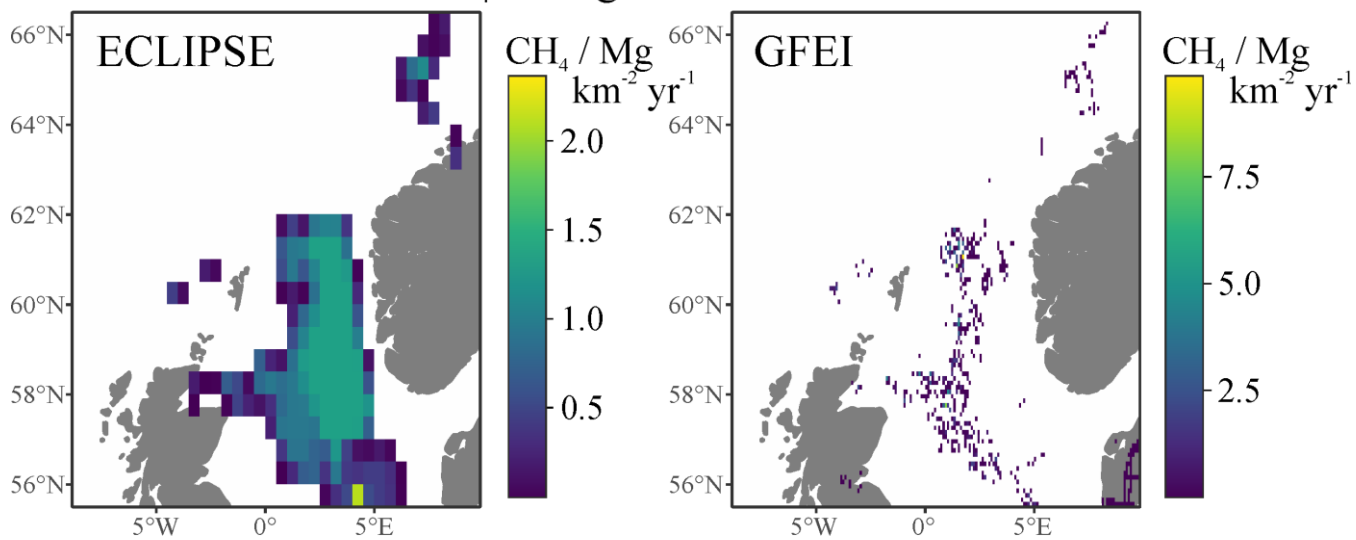


Figure D3. GFEI global CH₄ flaring emissions at 0.1° × 0.1° for 2019 (Scarpelli et al., 2020).

CH₄ flaring emissions



530 Figure D4. Left) ECLIPSE v5 CH₄ flaring emissions over the North Sea, at 0.5° × 0.5° for 2020 (Stohl et al., 2015). Right) GFEI CH₄ flaring emissions over the North Sea, at 0.1° × 0.1° for 2019 (Scarpelli et al., 2020).



ECLIPSE NO_x flaring emissions

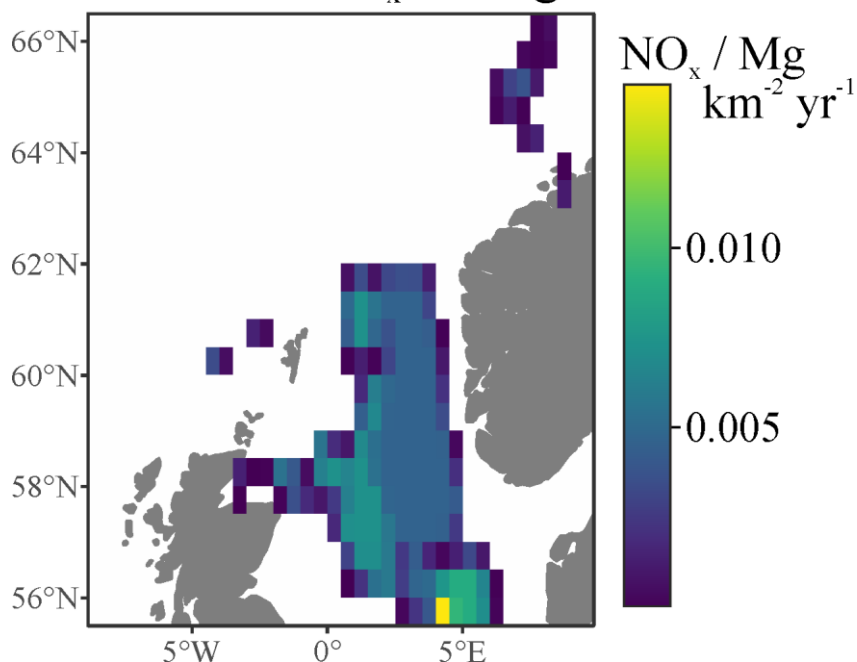


Figure D5. ECLIPSE v5 NO_x flaring emissions over the North Sea, at 0.5° × 0.5° for 2020 (Stohl et al., 2015).

535

ECLIPSE v5 NO_x:CH₄ ratio

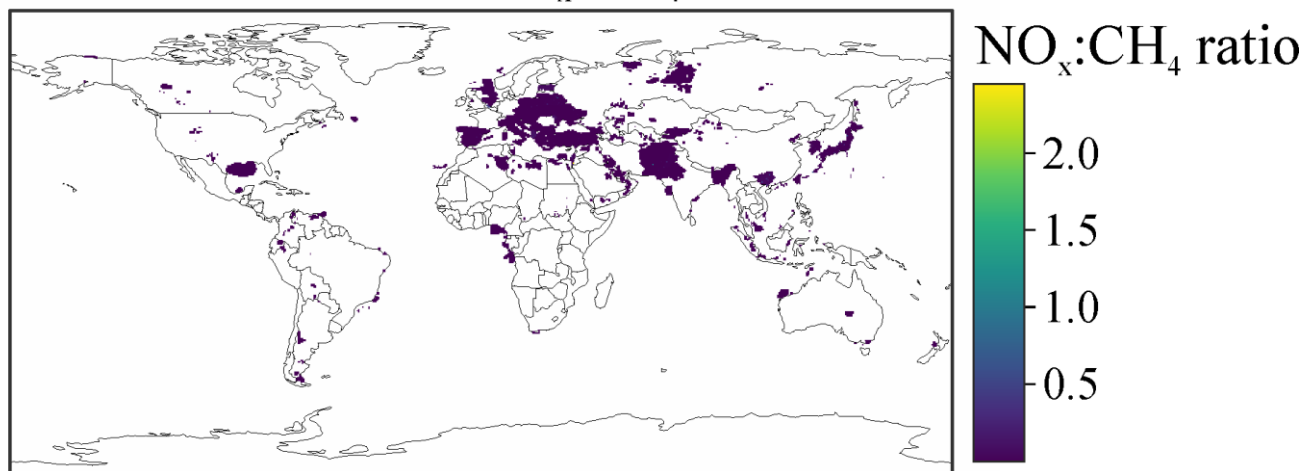
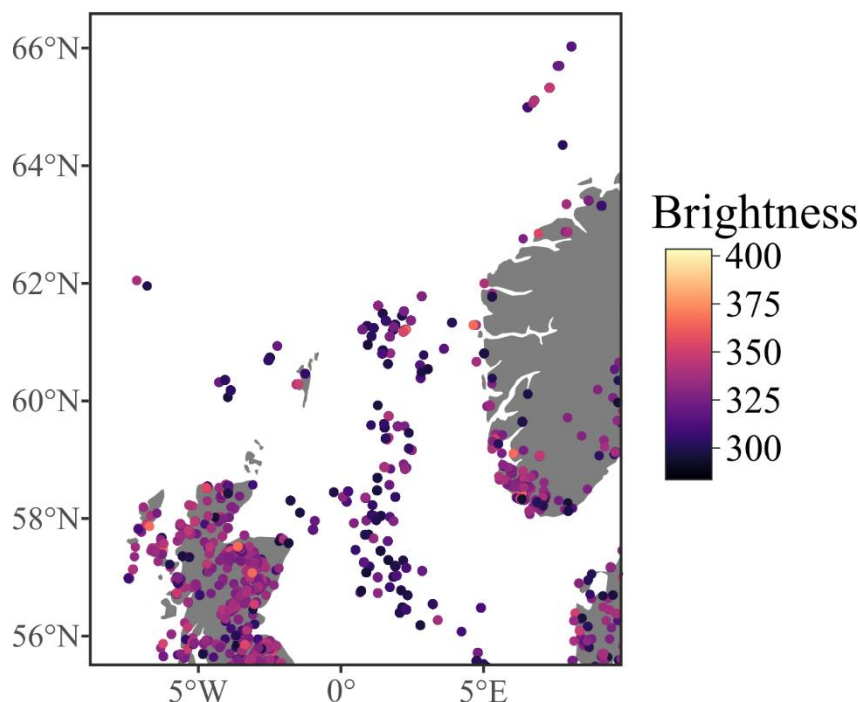


Figure D6. ECLIPSE v5 NO_x:CH₄ ratio, at 0.5° × 0.5° for 2020 (Stohl et al., 2015).



Appendix E: VIIRS data



540

Figure E1. Locations of active fire and thermal anomalies measured by the Moderate Resolution Imaging Spectroradiometer (MODIS) and Visible Infrared Imaging Radiometer Suite (VIIRS) Suomi-NPP between 01 September 2018 and 31 August 2019. Note that these data show the locations of observed thermal anomalies, which may or may not be indicative of natural gas flaring, although those over the North and Norwegian Seas are expected to be so. MODIS Collection 61 NRT Hotspot / Active Fire Detections MCD14DL distributed from NASA FIRMS. Available online <https://earthdata.nasa.gov/firms>; <https://doi.org/10.5067/FIRMS/MODIS/MCD14DL.NRT.0061NRT>. VIIRS 375 m Active Fire product VNP14IMG_T distributed from NASA FIRMS. Available online <https://earthdata.nasa.gov/firms>; https://doi.org/10.5067/FIRMS/VIIRS/VNP14IMG_T.NRT.002.

545

550



Data availability

Data from the AEOG and MOYA FAAM aircraft campaigns are available from the Centre for Environmental Data Analysis (CEDA) archive (<https://www.ceda.ac.uk>) at <https://catalogue.ceda.ac.uk/uuid/c94601501623483aa0a12e29ce99c0e0> (Crosier, 2022) and <https://catalogue.ceda.ac.uk/uuid/dd2b03d085c5494a8cbfc6b4b99ca702> (Nisbet, 2022) respectively. Please note that access to CEDA data sets and resources requires a free CEDA login account. This is in-line with funder policy and ensures appropriate use and citation of public data. GFEI emission grids are available for download from the Harvard Dataverse at <https://doi.org/10.7910/DVN/HH4EUM> (Scarpelli and Jacob, 2021). ECLIPSE global emission grids based on the GAINS model are publicly available from https://previous.iiasa.ac.at/web/home/research/researchPrograms/air/Global_emissions.html (IIASA, 2015).

Author contributions

JTS – Formal analysis, Methodology, Visualization, Writing – original draft preparation; **AF** – Formal analysis, Methodology, Writing – original draft preparation; **SW** – Formal analysis, Investigation, Visualization, Writing – original draft preparation; **PB** – Data curation, Investigation; **FS** – Data curation, Investigation; **JL** – Conceptualization, Investigation, Project administration, Funding acquisition; **RP** – Conceptualization, Investigation, Funding acquisition; **RB** – Investigation, Funding acquisition; **IC** - Investigation; **SM** – Investigation, Funding acquisition; **SJBB** – Data curation, Investigation; **SY** – Data curation, Investigation; **SS** – Writing – original draft preparation; **GA** – Conceptualization, Investigation, Methodology, Project administration, Writing – original draft preparation; Funding acquisition.

Competing interests

The contact author has declared the neither they nor their co-authors have any competing interests.

Acknowledgements

This work was supported by the Climate and Clean Air Coalition (CCAC) Oil and Gas Methane Science Studies (MSS) hosted by the United Nations Environment Programme. Funding was provided by the Environmental Defense Fund, the Oil and Gas Climate Initiative, the European Commission, and CCAC (Grant No.: DTIE19-020). The aircraft data used in this publication were collected as part of two projects: the Demonstration Of A Comprehensive Approach To Monitoring Emissions From Oil and Gas Installations (AEOG) project (Grant No.: NE/R01451X/1), and the Methane Observations and Yearly Assessment (MOYA) project (Grant No.: NE/N015835/1), both funded by the Natural Environment Research Council (NERC). We would like to thank Airtask Ltd. (who flew the aircraft), and all those involved in the operation and maintenance of the BAe-146-301 Atmospheric Research Aircraft, including FAAM, Avalon Aero, UK Research and Innovation (UKRI), and the University of Leeds. We also acknowledge the Offshore Petroleum Regulator for Environment and Decommissioning (OPRED) and Ricardo Energy & Environment for their involvement as project partners on the AEOG project. Any opinions, findings, conclusions, or recommendations expressed in this material are those of the author(s) and do not necessarily reflect the views of their respective institutions.

Financial support

This research was supported by the Natural Environment Research Council (Grant No.: NE/R01451X/1 and NE/N015835/1) and the Climate and Clean Air Coalition (Grant No.: DTIE19-020).



References

- Allen, D. T., Smith, D., Torres, V. M. and Saldaña, F. C.: Carbon dioxide, methane and black carbon emissions from upstream oil and gas flaring in the United States, *Curr. Opin. Chem. Eng.*, 13, 119-123, <https://doi.org/10.1016/j.coche.2016.08.014>, 2016.
- Anejionu, O. C. D., Whyatt, J. D., Blackburn, G. A. and Price, C. S.: Contributions of gas flaring to a global air pollution hotspot: Spatial and temporal variations, impacts and alleviation, *Atmos. Environ.*, 118, 184-193, <https://doi.org/10.1016/j.atmosenv.2015.08.006>, 2015.
- Barker, P. A., Allen, G., Gallagher, M., Pitt, J. R., Fisher, R. E., Bannan, T., Nisbet, E. G., Bauguitte, S. J.-B., Pasternak, D., Cliff, S., Schimpf, M. B., Mehra, A., Bower, K. N., Lee, J. D., Coe, H. and Percival, C. J.: Airborne measurements of fire emission factors for African biomass burning sampled during the MOYA campaign, *Atmos. Chem. Phys.*, 20, 15443-15459, <https://doi.org/10.5194/acp-20-15443-2020>, 2020.
- Cain, M., Warwick, N. J., Fisher, R. E., Lowry, D., Lanoisellé, M., Nisbet, E. G., France, J., Pitt, J., O'Shea, S., Bower, K. N., Allen, G., Illingworth, S., Manning, A. J., Bauguitte, S., Pisso, I. and Pyle, J. A.: A cautionary tale: A study of a methane enhancement over the North Sea, *J. Geophys. Res. Atmos.*, 122, 7630-7645, <https://doi.org/10.1002/2017JD026626>, 2017.
- Charles, J.-H. and Davis, M.: Flaring at FPSOs: Out of sight, but not out of mind, *Capterio*, <https://capterio.com/wp-content/uploads/2021/02/20210101-Flaring-at-FPSOs-out-of-sight-but-not-out-of-mind.pdf>, Last access: June 2022, 2021.
- Caulton, D. R., Shepson, P. B., Cambaliza, M. O. L., McCabe, D., Baum, E. and Stirm, B. H.: Methane destruction efficiency of natural gas flares associated with shale formation wells, *Environ. Sci. Technol.*, 48, 16, 9548-9554, <https://doi.org/10.1021/es500511w>, 2014.
- Corbin, D. J. and Johnson, M. R.: Detailed expressions and methodologies for measuring flare combustion efficiency, species emission rates, and associated uncertainties, *Ind. Eng. Chem. Res.*, 53, 19359-19369, <https://dx.doi.org/10.1021/ie502914k>, 2014.
- Crosier, J.: FAAM AEOG: Demonstration of comprehensive approach to monitoring atmospheric emissions from oil and gas installations, National Centre for Atmospheric Science (NCAS), CEDA Archive [data set], <https://catalogue.ceda.ac.uk/uuid/c94601501623483aa0a12e29ce99c0e0>, 2022.
- Dlugokencky, E. J., Myers, R. C., Lang, P. M., Masarie, K. A., Crotwell, A. M., Thoning, K. W., Hall, B. D., Elkins, J. W. and Steele, L. P.: Conversion of NOAA atmospheric dry air CH₄ mole fractions to a gravimetrically prepared standard scale, *J. Geophys. Res. Atmos.*, 110, <https://doi.org/10.1029/2005JD006035>, 2005.
- Elvidge C. D., Bazilian, M. D., Zhizhin, M., Ghosh, T., Baugh, K. and Hsu, F.-C.: The potential role of natural gas flaring in meeting greenhouse gas mitigation targets, *Energy Strateg. Rev.*, 20, 156-162, <https://doi.org/10.1016/j.esr.2017.12.012>, 2018.



- 620 EPA, AP-42: Fifth Edition Compilation of Air Emissions Factors, Volume 1: Stationary Point and Area Sources, Chapter 13.5
Industrial Flares, https://www.epa.gov/sites/default/files/2020-10/documents/13.5_industrial_flares.pdf, 2018.
- Fawole, O. G., Cai, X.-M. and MacKenzie, A. R.: Gas flaring and resultant air pollution: A review focusing on black carbon,
Environ. Poll., 216, 182-197, <https://doi.org/10.1016/j.envpol.2016.05.075>, 2016.
- France, J. L., Bateson, P., Dominutti, P., Allen, G., Andrews, S., Bauguitte, S., Coleman, M., Lachlan-Cope, T., Fisher, R. E.,
625 Huang, L., Jones, A. E., Lee, J., Lowry, D., Pitt, J., Purvis, R., Pyle, J., Shaw, J., Warwick, N., Weiss, A., Wilde, S.,
Witherstone, J. and Young, S.: Facility level measurement of offshore oil and gas installations from a medium-sized
airborne platform: Method development for quantification and source identification of methane emissions, Atmos.
Meas. Tech., 14, 71-88, <https://doi.org/10.5194/amt-14-71-2021>, 2021.
- Foulds, A., Allen, G., Shaw, J. T., Bateson, P., Barker, P. A., Huang, L., Pitt, J. R., Lee, J. D., Wilde, S. E., Dominutti, P.,
630 Purvis, R. M., Lowry, D., France, J. L., Fisher, R. E., Fiehn, A., Pühl, M., Bauguitte, S. J.-B., Conley, S. A., Smith,
M. L., Lachlan-Cope, T., Pisso, I. and Schwietzke, S.: Quantification and assessment of methane emissions from
offshore oil and gas facilities on the Norwegian continental shelf, Atmos. Chem. Phys., 22, 4303-4322,
<https://doi.org/10.5194/acp-22-4303-2022>, 2022.
- Graham, A. M., Pope, R. J., McQuaid, J. B., Pringle, K. P., Arnold, S. R., Burno, A. G., Moore, D. P., Harrison, J. J.,
635 Chipperfield, M. P., Rigby, R., Sanchez-Marroquin, A., Lee, J., Wilde, S., Siddans, R., Kerridge, B. J., Ventress, L.
J. and Latter, B. G.: Impact of the June 2018 Saddleworth Moor wildfires on air quality in northern England, Environ.
Res. Commun., 2, 031001, <https://doi.org/10.1088/2515-7620/ab7b92>, 2020.
- Gvakharia, A., Kort, E. A., Brandt, A., Peischl, J., Ryerson, T. B., Schwarz, J. P., Smith, M. L. and Sweeney, C.: Methane,
black carbon, and ethane emissions from natural gas flares in the Bakken Shale, North Dakota, Env. Sci. Technol.,
640 51, 5317-5325, <http://dx.doi.org/10.1021/acs.est.6b05183>, 2017.
- Hodnebrog, Ø., Dalsøren, S. B. and Myhre, G.: Lifetimes, direct and indirect radiative forcing, and global warming potentials
of ethane (C₂H₆), propane (C₃H₈), and butane (C₄H₁₀), Atmos. Sci. Lett., 19, e804, <https://doi.org/10.1002/asl.804>,
2018.
- IEA, International Energy Agency, Offshore Energy Outlook, [https://iea.blob.core.windows.net/assets/f4694056-8223-4b14-
645 b688-164d6407bf03/WEO_2018_Special_Report_Offshore_Energy_Outlook.pdf](https://iea.blob.core.windows.net/assets/f4694056-8223-4b14-b688-164d6407bf03/WEO_2018_Special_Report_Offshore_Energy_Outlook.pdf), Last accessed September 2022,
2018.
- IEA, International Energy Agency, Flaring Emissions, Paris, <https://www.iea.org/reports/flaring-emissions>, Last accessed May
2022, 2021.
- IIASA, International Institute for Applied Systems Analysis, ECLIPSE v5a global emission fields [data set],
650 <https://previous.iiasa.ac.at/web/home/research/researchPrograms/air/ECLIPSEv5a.html>, 2015.
- IPCC, Intergovernmental Panel on Climate Change, Climate Change 2021: The Physical Science Basis, Contribution of
Working Group I to the Sixth Assessment Report of the Intergovernmental Panel on Climate Change [Masson-
Delmotte, V., Zhai, P., Pirani, A., Connors, S. L., Péan, C., Berger, S., Caud, N., Chen, Y., Goldfarb, L., Gomis, M.



- I., Huang, M., Leitzell, K., Lonnoy, E., Matthews, J. B. R., Maycock, T. K., Waterfield, T., Yelekçi, O., Yu, R. and
655 Zhou, B. (eds.)], Cambridge University Press, 2021.
- Ismail, I. S. and Umukoro, G. E.: Global impact of gas flaring, *Energy and Power Engineering*, 4, 290-302,
<https://doi.org/10.4236/epe.2012.44039>, 2012
- Jatale, A., Smith, P. J., Thornock, J. N., Smith, S. T. and Hradisky, M.: A validation of flare combustion efficiency predictions
from large eddy simulations, *J. Verif. Valid. Uncert.*, 1, 021001, <https://doi.org/10.1115/1.4031141>, 2016.
- 660 Johnson, M. R. and Kostiuk, L. W.: A parametric model for the efficiency of a flare in crosswind, *P. Combust. Inst.*, 29, 1943-
1950, [https://doi.org/10.1016/S1540-7489\(02\)80236-X](https://doi.org/10.1016/S1540-7489(02)80236-X), 2002.
- Kahforoshan, D., Fatehifar, E., Babalou, A. A., Ebrahimin, A. R., Elkamel, A. and Soltanmohammadzadeh, J. S.: Modelling
and evaluation of air pollution from a gaseous flare in an oil and gas processing area, In *Selected Papers from the
WSEAS Conferences in Spain*, 180-186, 2008.
- 665 Knighton, W. B., Herndon, S. C., Franklin, J. F., Wood, E. C., Wormhoudt, J., Brooks, W., Fortner, E. C. and Allen, D. T.:
Direct measurement of volatile organic compound emissions from industrial flares using real-time online techniques:
Proton transfer reaction mass spectrometry and tunable infrared laser differential absorption spectroscopy, *Ind. Eng.
Chem. Res.*, 51, 39, 12674-12684, <https://doi.org/10.1021/ie202695v>, 2012.
- Lee, J. D., Moller, S. J., Read, K. A., Lewis, A. C., Mendes, L. and Carpenter, L. J.: Year-round measurements of nitrogen
670 oxides and ozone in the tropical North Atlantic marine boundary layer, *J. Geophys. Res. Atmos.*, 114,
<https://doi.org/10.1029/2009JD011878>, 2009.
- Lyon, D. R., Hmiel, B., Gautam, R., Omara, M., Roberts, K. A., Barkley, Z. R., Davis, K. J., Miles, N. L., Monteiro, V. C.,
Richardson, S. J., Conley, S., Smith, M. L., Jacob, D. J., Shen, L., Varon, D. J., Deng, A., Rudelis, X., Sharma, N.,
Story, K. T., Brandt, A. R., Kang, M., Kort, E. A., Marchese, A. J. and Hamburg, S. P.: Concurrent variation in oil
675 and gas methane emissions and oil price during the COVID-19 pandemic, *Atmos. Chem. Phys.*, 21, 6605-6626,
Atmos. Chem. Phys., 21, 6605-6626, 2021, <https://doi.org/10.5194/acp-21-6605-2021>, 2021.
- Myhre, G., Shindell, D., Bréon, F.-M., Collins, W., Fuglestedt, J., Huang, J., Koch, D., Lamarque, J.-F., Lee, D., Mendoza,
B., Nakajima, T., Robock, A., Stephens, G., Takemura, T. and Zhang, H.: Anthropogenic and natural radiative
forcing, In: *Climate Change 2013: The Physical Science Basis, Contribution of Working Group I to the Fifth
680 Assessment Report of the Intergovernmental Panel on Climate Change* [Stocker, T. F., Qin, D., Plattner, G.-K.,
Tignor, M., Allen, S. K., Boschung, J., Nauels, A., Xia, Y., Bex, V. and Midgley, P. M. (eds.)], Cambridge University
Press, Cambridge, United Kingdom and New York, NY, USA, 2013.
- Nara, H., Tanimoto, H., Tohjima, Y., Mukai, H., Nojiri, Y. and Machida, T.: Emissions of methane from offshore oil and gas
platforms in Southeast Asia, *Sci. Rep.*, 4, 6503, <https://doi.org/10.1038/srep06503>, 2014.
- 685 Nisbet, Methane Observations and Yearly Assessments (MOYA), Natural Environment Research Council (NERC), CEDA
Archive [data set], <https://catalogue.ceda.ac.uk/uuid/dd2b03d085c5494a8cbfc6b4b99ca702>, 2022.



- OGA, Oil & Gas Authority, Emissions Monitoring Report, https://www.nstauthority.co.uk/media/7809/emissions-report_141021.pdf, Last access: May 2022, 2021.
- 690 Olivier, J. G. I., Janssens-Maenhout, G. and Peters, J. A. H. W.: Trends in global CO₂ emissions, PBL Netherlands Environmental Assessment Agency, 16-17, 2013.
- O'Shea, S. J., Bauguitte, S. J.-B., Gallagher, M. W., Lowry, D. and Percival, C. J.: Development of a cavity-enhanced absorption spectrometer for airborne measurements of CH₄ and CO₂, *Atmos. Meas. Tech.*, 6, 1095-1109, <https://doi.org/10.5194/amt-6-1095-2013>, 2013.
- 695 Palmer, P. I., O'Doherty, S., Allen, G., Bower, K., Bösch, H., Chipperfield, M. P., Connors, S., Dhomse, S., Feng, L., Finch, D. P., Gallagher, M. W., Gloor, E., Gonzi, S., Harris, N. R. P., Knappett, D., Jones, R. L., Le Breton, M., Lunt, M. F., Manning, A. J., Matthiesen, S., Muller, J. B. A., Mullinger, N., Nemitz, E., O'Shea, S., Parker, R. J., Percival, C. J., Pitt, J., Riddick, S. N., Rigby, M., Sembhi, H., Siddans, R., Skelton, R. L., Smith, P., Sonderfeld, H., Stanley, K., Stavert, A. R., Wenger, A., White, E., Wilson, C. and Young, D.: A measurement-based verification framework for UK greenhouse gas emissions: an overview of the Greenhouse gAs Uk and Global Emissions (GAUGE) project, *Atmos. Chem. Phys.*, 18, 11753-11777, <https://doi.org/10.5194/acp-18-11753-2018>, 2018.
- 700 Pitt, J. R., Le Breton, M., Allen, G., Percival, C., Gallagher, M. W., Bauguitte, S. J.-B., O'Shea, S. J., Muller, J. B. A., Zahniser, M. S., Pyle, J. and Palmer, P. I.: The development and evaluation of airborne in situ N₂O and CH₄ sampling using a quantum cascade laser absorption spectrometer (QCLAS), *Atmos. Meas. Tech.*, 9, 63-77, <https://doi.org/10.5194/amt-9-63-2016>, 2016.
- 705 Pitt, J. R., Allen, G., Bauguitte, S. J.-B., Gallagher, M. W., Lee, J. D., Drysdale, W., Nelson, B., Manning, A. J. and Palmer, P. I.: Assessing London CO₂, CH₄ and CO emissions using aircraft measurements and dispersion modelling, *Atmos. Chem. Phys.*, 19, 8931-8945, <https://doi.org/10.5194/acp-19-8931-2019>, 2019.
- Plant, G., Kort, E. A., Brandt, A. R., Chen, Y., Fordice, G., Gorchov Negron, A., Schwietzke, S., Smith, M. and Zavala-Araiza, D.: Inefficient and unlit natural gas flares both emit large quantities of methane, *Science*, <https://doi.org/10.1126/science.abq0385>, 2022.
- 710 Pühl, M., Roiger, A., Fiehn, A., Gorchov Negron, A. M., Kort, E. A., Schwietzke, S., Pisso, I., Foulds, A., Lee, J., France, J. L., Jones, A. E., Lowry, D., Fisher, R. E., Huang, L., Shaw, J., Bateson, P., Andrews, S., Young, S., Dominutti, P., Lachlan-Cope, T., Weiss, A. and Allen, G.: Aircraft-based mass balance estimate of methane emissions from offshore gas facilities in the Southern North Sea, *in prep.*
- 715 Riddick, S. N., Mauzerall, D. L., Celia, M., Harris, N. R. P., Allen, G., Pitt, J., Staunton-Sykes, J., Forster, G. L., Kang, M., Lowry, D., Nisbet, E. G. and Manning, A. J.: Methane emissions from oil and gas platforms in the North Sea, *Atmos. Chem. Phys.*, 19, 9787-9796, <https://doi.org/10.5194/acp-19-9787-2019>, 2019.
- 720 Saunio, M., Stavert, A. R., Poulter, B., Bousquet, P., Canadell, J. G., Jackson, R. B., Raymond, P. A., Dlugokencky, E. J., Houweling, S., Patra, P. K., Ciais, P., Arora, V. K., Bastviken, D., Bergamaschi, P., Blake, D. R., Brailsford, G., Bruhwiler, L., Carlson, K. M., Carrol, M., Castaldi, S., Chandra, N., Crevoisier, C., Crill, P. M., Covey, K., Curry, C.



- 725 L., Etiope, G., Frankenberg, C., Gedney, N., Hegglin, M. I., Höglund-Isaksson, L., Hugelius, G., Ishizawa, M., Ito, A., Janssens-Maenhout, G., Jensen, K. M., Joos, F., Kleinen, T., Krummel, P. B., Langenfelds, R. L., Laruelle, G. G., Liu, L., Machida, T., Maksyutov, S., McDonald, K. C., McNorton, J., Miller, P. A., Melton, J. R., Morino, I., Müller, J., Murguía-Flores, F., Naik, V., Niwa, Y., Noce, S., O'Doherty, S., Parker, R. J., Peng, C., Peng, S., Peters, G. P., Prigent, C., Prinn, R., Ramonet, M., Regnier, P., Riley, W. J., Rosentreter, J. A., Segers, A., Simpson, I. J., Shi, H., Smith, S. J., Steele, L. P., Thornton, B. F., Tian, H., Tohjima, Y., Tubiello, F. N., Tsuruta, A., Viovy, N., Voulgarakis, A., Weber, T. S., van Weele, M., van der Werf, G. R., Weiss, R. F., Worthy, D., Wunch, D., Yin, Y., Yoshida, Y., Zhang, W., Zhang, Z., Zhao, Y., Zheng, B., Zhu, Q., Zhu, Q. and Zhuang, Q.: The global methane budget 2000-2017, *Earth Syst. Sci. Data*, 12, 1561-1623, <https://doi.org/10.5194/essd-12-1561-2020>, 2020.
- 730 Scarpelli, T. R., Jacob, D. J., Maasackers, J. D., Sulprizio, M. P., Sheng, J.-X., Rose, K., Romeo, L., Worden, J. R. and Janssens-Maenhout, G.: A global gridded ($0.1^\circ \times 0.1^\circ$) inventory of methane emissions from oil, gas, and coal exploitation based on national reports to the United Nations Framework Convention on Climate Change, *Earth Syst. Sci. Data*, 12, 563-575, <https://doi.org/10.5194/essd-12-563-2020>, 2020.
- 735 Scarpelli, T. R. and Jacob, D. J.: Global Fuel Exploitation Inventory (GFEI), Harvard Dataverse [data set], <https://doi.org/10.7910/DVN/HH4EUM>, 2021.
- Schwietzke, S., Griffin, W. M., Matthews, H. S. and Bruhwiler, L. M. P.: Natural gas fugitive emissions rates constrained by global atmospheric methane and ethane, *Environ. Sci. Technol.*, 48, 7714-7722, <https://doi.org/10.1021/es501204c>, 2014.
- 740 Shaw, J. T., Allen, G., Barker, P., Pitt, J. R., Pasternak, D., Bauguitte, S. J.-B., Lee, J., Boewer, K. N., Daly, M. C., Lunt, M. F., Ganesan, A. L., Vaughan, A. R., Chibesakunda, F., Lambakasa, M., Fisher, R. E., France, J. L., Lowry, D., Palmer, P. I., Metzger, S., Parker, R. J., Gedney, N., Bateson, P., Cain, M., Lorente, A., Borsdorff, T. and Nisbet, E. G.: Large methane emission fluxes observed from tropical wetlands in Zambia, *Glob. Biogeochem. Cy.*, 36, e2021GB007261, <https://doi.org/10.1029/2021GB007261>, 2022.
- 745 Sherwood, O. A., Schwietzke, S., Arling, V. A. and Etiope, G.: Global inventory of gas geochemistry data from fossil fuel, microbial and burning sources, version 2017, *Earth. Syst. Sci. Data*, 9, 639-656, <https://doi.org/10.5194/essd-9-639-2017>, 2017.
- 750 Stohl, A., Aamaas, B., Amann, M., Baker, L. H., Belloiun, N., Berntsen, T. K., Boucher, O., Cherian, R., Collins, W., Daskalakis, N., Dusinska, M., Eckhardt, S., Fuglestedt, J. S., Harju, M., Heyes, C., Hodnebrog, Ø., Hao, J., Im, U., Kanakidou, M., Klimont, Z., Kupiainen, K., Law, K. S., Lund, M. T., Maas, R., MacIntosh, C. R., Myhre, G., Myriokefalitakis, S., Olivié, D., Quaas, J., Quennehen, B., Raut, J.-C., Rumbold, S. T., Samset, B. H., Schulz, M., Seland, Ø., Shine, K. P., Skeie, R. B., Wang, S., Yttri, K. E. and Zhu, T.: Evaluating the climate and air quality impacts of short-lived pollutants, *Atmos. Chem. Phys.*, 15, 10529-10566, <http://www.atmos-chem-phys.net/15/10529/2015/>, 2015.



- 755 Tans, P., Zhao, C. and Kitzis, D.: The WMO Mole Fraction Scales for CO₂ and other greenhouse gases, and uncertainty of the atmospheric measurements, in: 15th WMO/IAEA Meeting of Experts on Carbon Dioxide, Other Greenhouse Gases, and Related Tracer Measurement Techniques, Jena, Germany, 2009
- Torres, V. M., Herndon, S., Kodosh, Z. and Allen, D. T.: Industrial flare performance at low flow conditions: 1. Study overview, *Ind. Eng. Chem. Res.*, 51, 39, 12559-12568, <https://doi.org/10.1021/ie202674t>, 2012a.
- Torres, V. M., Herndon, S. and Allen, D. T.: Industrial flare performance at low flow conditions: 2. Steam- and air-assisted
760 flares, *Ind. Eng. Chem. Res.*, 51, 39, 12569-12576, <https://doi.org/10.1021/ie202675f>, 2012b.
- Torres, V. M., Herndon, S., Wood, E., Al-Fadhli, F. and Allen, D. T.: Emissions of nitrogen oxides from flares operating at low flow conditions, *Ind. Eng. Chem. Res.*, 51, 39, 12600-12605, <https://doi.org/10.1021/ie300179x>, 2012c.
- Turner, A. J., Frankenberg, C., Wennberg, P. O. and Jacob, D. J.: Ambiguity in the causes for decadal trends in atmospheric methane and hydroxyl, *P. Natl. Acad. Sci. USA*, 114, 5367-5372, <https://doi.org/10.1073/pnas.1616020114>, 2017.
- 765 United Nations, Kyoto Protocol to the United Nations Framework Convention on Climate Change, <https://unfccc.int/resource/docs/convkp/kpeng.pdf>, 1998.
- Wilde, S. E.: Atmospheric emissions from the UK oil and gas industry, PhD thesis, University of York, 2021a.
- Wilde, S. E., Dominutti, P. A., Allen, G., Andrews, S. J., Bateson, P., Bauguitte, S. J.-B., Burton, R. R., Colfescu, I., France, J., Hopkins, J. R., Huang, L., Jones, A. E., Lachlan-Cope, T., Lee, J. D., Lewis, A. C., Mobbs, S. D., Weiss, A.,
770 Young, S. and Purvis, R. M.: Speciation of VOC emissions related to offshore North Sea oil and gas production, *Atmos. Chem. Phys.*, 21, 3741-3762, <https://doi.org/10.5194/acp-21-3741-2021>, 2021b.
- World Bank, Global Gas Flaring Tracker Report, <https://thedocs.worldbank.org/en/doc/1f7221545bf1b7c89b850dd85cb409b0-0400072021/original/WB-GGFR-Report-Design-05a.pdf>, Last access: June 2022, 2021.
- 775 Xiao, Y., Logan, J. A., Jacob, D. J., Hudman, R. C., Yantosca, R. and Blake, D. R.: Global budget of ethane and regional constraints on US sources, *J. Geophys. Res. Atmos.*, 113, D21, <https://doi.org/10.1029/2007JD009415>, 2008.
- Yokelson, R. J., Andreae, M. O. and Akagi, S. K.: Pitfalls with the use of enhancement ratios or normalized excess mixing ratios measured in plumes to characterize pollution sources and aging, *Atmos. Meas. Tech.*, 6, 2155-2158, <http://www.atmos-meas-tech.net/6/2155/2013/>, 2013.